AD-A035 179 TENNESSEE UNIV SPACE INST TULLAHOMA DEPT OF METALLUR--ETC F/G 11/6
INVESTIGATIONS INTO THE MECHANISMS OF THERMAL CYCLING DAMAGE IN--ETC(U)
DEC 76 M K WHITE, M A WRIGHT N00014-75-C-0352
UNCLASSIFIED MET-E-761 NL

1 OF 1
ADA035179

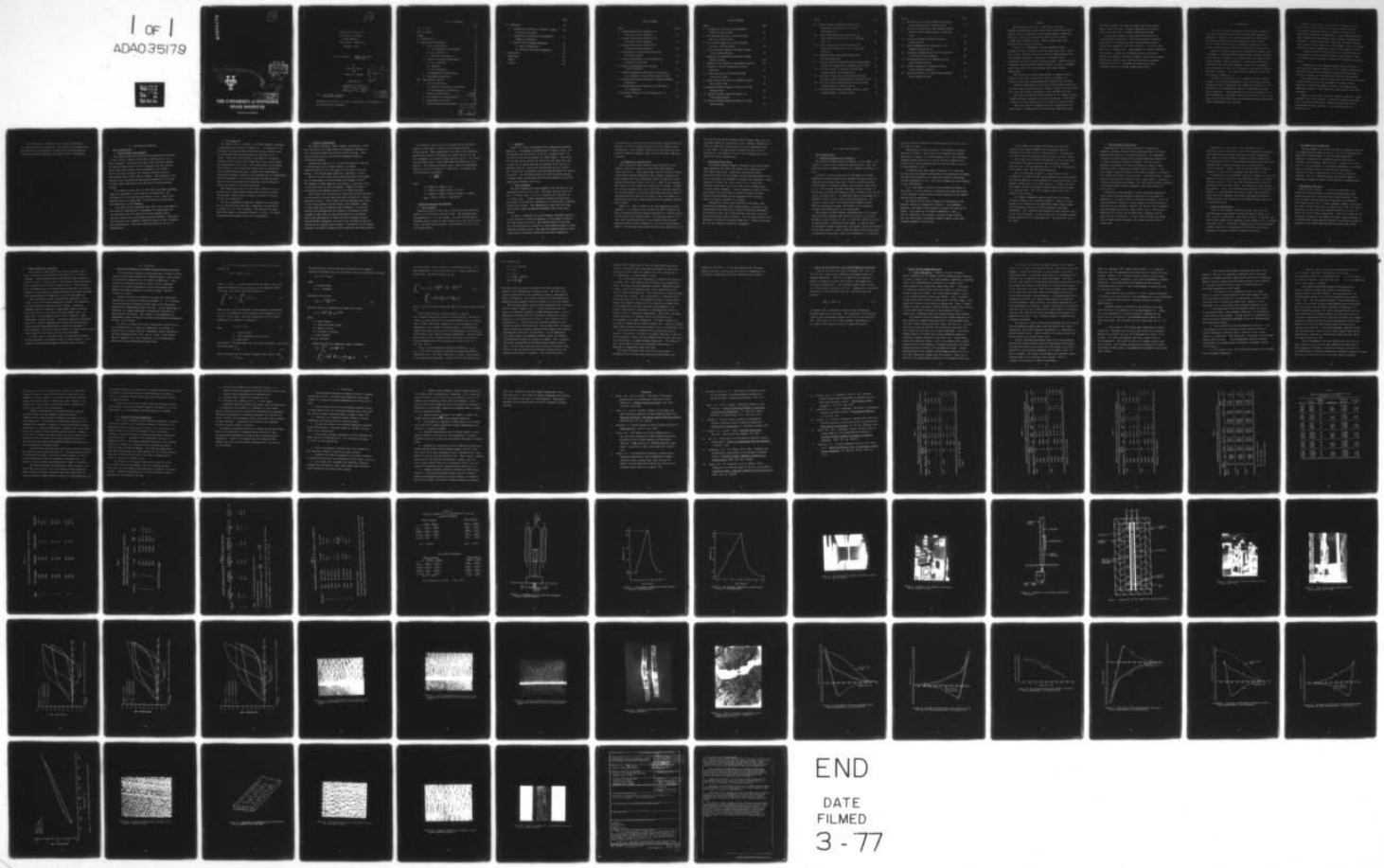

END

DATE
FILMED
3-77

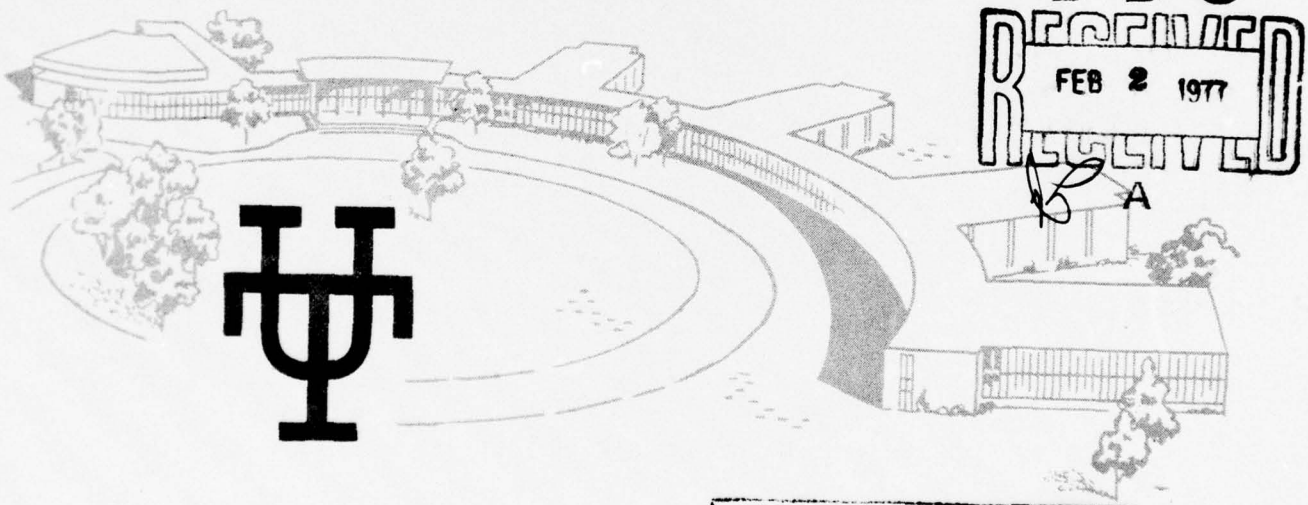

THE UNIVERSITY of TENNESSEE SPACE INSTITUTE

Tullahoma, Tennessee

(12)

Investigations into the Mechanisms of Thermal Cycling Damage in Metal Matrix Composites

December, 1976

Contract Number N00014-75-C-0352
NR 031-760

by

Marvis K. White
and
Maurice A. Wright

Submitted to

Department of the Navy
Office of Naval Research
Washington, D.C. 20360

Attn: W.C. Rauch, Director
Metallurgy Program

TABLE OF CONTENTS

	Page
List of Tables	1
List of Figures	2
Summary	5
I. Introduction	7
II. Experimental Techniques	10
1. Inert Cycling Tests	10
a) Test Materials and Specimens	10
b) Test Apparatus	11
c) Property Determination	12
2. Composite Expansion Measurements	13
a) Test Specimens	13
b) Apparatus	14
c) Test Procedures	14
3. Low Temperature Cycling Tests	15
4. Superimposed Load Tests	16
III. Experimental Results	17
1. Inert Cycling Tests	17
a) Mechanical Properties and Density	17
b) Metallographic Observations	20
2. Expansion Measurements	21
3. Low Temperature Cycling Tests	22
4. Superimposed Load Tests	22
5. Carbon-Aluminum Cycling Tests	23

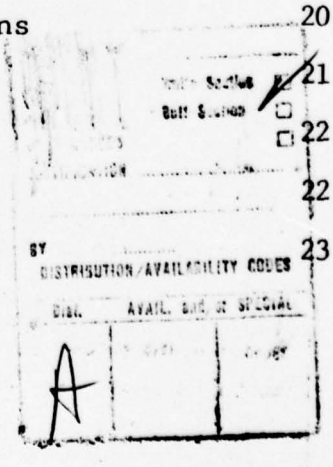

		Page
IV.	Discussion	24
	1. Theoretical Evaluation of Thermal Cycling Stresses and Strains	24
	2. Comparison of Theoretical and Measured Composite Expansions	31
	3. Thermal Cycling Damage Mechanisms	32
	a) Matrix Degradation	32
	b) Interface and Fiber Degradation	38
V.	Conclusions	40
	References	43
	Tables	46
	Figures	56

LIST OF TABLES

Table		Page
1.	Measured Mechanical Properties of 6061 Matrix B-Al Composite	46
2.	Measured Mechanical Properties of 2024 Matrix B-Al Composite	47
3.	Measured Mechanical Properties of 1100 Matrix B-Al Composite	48
4.	Experimental Data for Extracted 2 Inch Long Boron Fibers	49
5.	Density Measurements of As-Received and Thermally Cycled B-Al	50
6.	6061 Al-B Thermally Cycled Between -100°C and +275°C	51
7.	Measured Mechanical Properties of 6061 Matrix B-Al Composites Cycled Under External Loads	52
8.	Measured Mechanical Properties of Carbon-Aluminum Composites	53
9.	Measured Mechanical Properties of 2024 Matrix C-Al Composites.	54
10.	Dimension Changes in C-Al Specimens Due to Cycling	55

LIST OF FIGURES

Figure		Page
1.	A Diagram of the Controlled Atmosphere Thermal Cycling Furnace	56
2.	The Specimen Temperature During Thermal Cycling, 6 Minutes/Cycle	57
3.	The Specimen Temperature During Thermal Cycling, 12 Minutes/Cycle	58
4.	An Instrumented Composite Specimen Gripped in the Tensile Machine	59
5.	Apparatus for Expansion Measurement During Thermal Cycling	60
6.	Diagram of the Expansion Measurement Apparatus	61
7.	Diagram of the Low Temperature Cycling Apparatus	62
8.	Furnace Unit Used for Thermal Cycling Under Static Load	63
9.	Water Cooled Grips Used for Thermal Cycling Under Static Load	64
10.	Measured Thermal Expansion Behavior of 1100 Aluminum-Boron	65
11.	Measured Thermal Expansion Behavior of 2024 Aluminum-Boron	66
12.	Measured Thermal Expansion Behavior of 6061 Aluminum-Boron	67

Figure Page

13. Surface Appearance Before and After Low Temperature Cycling of 27 v/o, 0.04 Thick-6061 Al-B 68
14. Surface Appearance Before and After Low Temperature Cycling of 45 v/o, 0.045 Thick 6061 Al-B 69
15. Surface Appearance Before and After Low Temperature Cycling of 45 v/o, 0.08, Thick 6061 Al-B 70
16. Thermally Cycled Transverse Carbon-2024 Aluminum Specimens 71
17. Crack in Surface of Thermally Cycled Longitudinal Carbon 2024 Aluminum at a Magnification of 350 72
18. The Matrix Stress on Thermally Cycled 2024 Aluminum-Boron, 12 Minutes/cycle 73
19. The Matrix Stress-Strain Curve During Thermal Cycling of 2024 Aluminum-Boron, 12 Minutes/cycle 74
20. The Creep Strain During Thermal Cycling of 2024 Aluminum-Boron, 12 Minutes/cycle 75
21. The Fiber Stress During Thermal Cycling of 2024 Aluminum-Boron, 12 Minutes/cycle 76

Figure		Page
22.	The Matrix Stress During Thermal Cycling of 2024 Aluminum-Boron, 6 Minutes/Cycle	77
23.	The Matrix Stress-Strain Curve During Thermal Cycling of 2024 Aluminum-Boron, 6 Minutes/Cycle	78
24.	Calculated Composite Thermal Extension, 6 Minutes/Cycle	79
25.	Surface Roughening and Cracking of B-Al Thermally Cycled in Air	80
26.	Diagramatic Representation of the Surface of a Thermally Cycled Specimen	81
27.	The Spheroidazation of a Thermally Cycled Boron-Aluminum Surface	82
28.	Surface Disruption of Thermally Cycled Carbon-Aluminum Composite	83
29.	Reaction Products on a Boron Fiber Extracted After Thermal Cycling	84

Summary

The mechanical properties of 6061, 2024, and 1100 aluminum reinforced with boron fibers were measured after 6000 thermal cycles in argon and in air between ambient temperature and 425°c. The cyclic periods used were 6 and 12 minutes in argon and 12 minutes in air. Fiber strengths were also measured before and after cycling.

Little or no longitudinal strength degradation was evidenced by those materials cycled in argon while those cycled in air under otherwise identical conditions showed greater than 50% strength reductions. Cycling in air produced lower transverse strengths than did cycling in argon. Fibers extracted from argon cycled specimens showed little or no loss of strength while those from air cycled specimens had large strength degradations.

The stresses and strains generated in a composite during thermal cycling were calculated in order to determine the nature of the strains producing matrix ratcheting and cracking.

Expansion measurements of the three boron-aluminum composites were made during thermal cycling in order to check the calculations and to provide further information on the deformation process.

The effect of applied tensile stresses on the thermal cycling response of boron-aluminum in air was investigated. Tests using a variety of loads showed little or no effect of applied stress.

Also, the effect of reducing the cyclic temperatures was investigated. Keeping the cyclic period and temperature range

the same as before, the lower and upper limits were shifted down to -100°c and 275°c. Matrix roughening was evidenced after 3000 cycles but no strength reduction was found.

In addition, thermal cycling tests were conducted on carbon-aluminum composites. 2024 aluminum matrix composites containing 27 v/o Thornel-50 fibers were thermally cycled between room temperature and 365°c and 425°c. All tests were done with a 3 minute cycle. Large amounts of surface roughening and cracking, a large but misleading decrease in flexual modulus, no change in the tensile modulus, and tensile strength reductions as high as about 70% were found using a maximum temperature of 425°c. No damage was indicated in those specimens cycled to a maximum temperature of 365°c.

I. Introduction

One of the principal advantages of metal matrix composites over those with polymeric matrices is their high temperature capability. However, all of these materials have been shown to be adversely affected in varying degrees by either static [1,2] or cyclic [3-6] elevated temperature exposures in air, often resulting in very substantial reductions in service life.

Among the effects experienced are dimensional changes such as bending or twisting, surface roughening and cracking, internal void formation, reactions of the phases with each other or with the environment, matrix delamination, fiber-matrix interface disruption, and even fiber breakage. These, either seperately or in combination, result in a decrease in the tensile, flexural, and shear strengths, the failure strain, Poisson's ratios and the fracture toughness [4].

A number of mechanisms such as chemical reaction, thermal fatigue, stress corrosion cracking, creep, precipitate particle segregation, grain coarsening, and others may contribute to the production of the detrimental effects of temperature on metal matrix composites. Their operation is often very complex due to the heterogeneous, anisotropic nature of the material, and to the fact that very often more than one mechanism function concurrently, eigher independently or conjointly.

During the past year, the University of Tennessee Space Institute has been carrying out a diverse program of work in continuing to study the effects of thermal cycling on the properties of metal-matrix composites. It was conjectured that fiber oxidation was the principal direct cause of reduced axial strengths. To help verify this, 1100, 2024, and 6061 aluminum-boron composites were subjected to 6000 thermal cycles in an argon environment between temperature limits of near ambient to 425°c.

A computer analysis of the stresses and strains present in such composites during thermal cycling was undertaken in order to determine how they operate to produce the observed detrimental effects.

Measurements of the thermal expansion and contraction of boron-aluminum composites during 3, 6 and 12 minute thermal cycles were made to check the calculated stresses and strains and to provide information on the deformation behavior and processes.

Other experimental studies investigated the effects of applied tensile stresses on the rate and amount of thermal cycling degradation and also the effect of lower cyclic temperatures. Temperature limits of -100°c and +275°c were used in the latter experiment.

Thermal cycling tests on another composite material, carbon-aluminum, were also conducted. Carbon-2024 aluminum containing 27 v/o Thornel-50 fibers were thermally cycled between room temperature and 365°c and 425°c. All tests were done at 3 minutes/cycle.

The experimental techniques used in these investigations are discussed in the next section. The results of the experiments described above are presented in Section III and the discussion and conclusions are presented in Sections IV and V respectively.

II. Experimental Technique

1. Inert Cycling Tests

a. Test materials and specimens

The composite materials used in this investigation consisted of three types of aluminum alloy matrix reinforced with 45 v/o boron filaments. The alloys were 6061, 2024, and 1100 aluminum. The boron filaments were 5.8 mil in diameter with the exception of the 6061 alloy material which contained 4.0 mil fibers. This 4-mil fibers composite was received ready-cut from the NASA Marshall Space Flight Center, Alabama. The remainder of the materials were obtained from the Amercom Corporation in the form of sheet panels fabricated by the hot press diffusion bonding process.

The composite panels were cut by electric discharge machining (EDM) into specimens 6 inches long by 0.5 inches wide. The thickness of all the materials was about 0.5 inch. Half of the specimens were cut longitudinal to the filaments and the other half transverse to the filaments.

Four groups of B-Al specimens were used in this investigation. Each group was comprised of 12 specimens, two longitudinal and two transverse taken from each of the three material types. One group served as an as-received condition reference. The second and third group were thermally cycled in argon at 6 and 12 minutes/cycle respectively. The fourth group was cycled in air at 12 minutes/cycle.

b. Test apparatus

The furnace used to thermally cycle these composite specimens is diagramatically depicted in Figure (1) . It consisted of an electrical resistance heated cylindrical furnace movable along its axis about which were positioned the specimens to be cycled. These were mounted against the sides of a hexagonal stainless steel cooling block through which water flowed during the cooling part of the cycle. The cooling block and specimens were sealed in a Vycor glass tube which could be evacuated of air and back-filled with a gas. Cooling was accomplished by pulling the furnace up from over the specimens with an automatically controlled gearmotor, by circulating water through the steel block on which the specimens were mounted, and by blowing air around the outside of the glass enclosure.

The temperature curves for the 6 and 12 minute cycles, as measured by a chromel-alumel thermocouple positioned against one specimen, midway along its length, are shown in Figures (2) and (3) respectively.

The inert atmosphere cycling was conducted by evacuating the air from the glass tube with a mechanical vacuum pump to a pressure of 1 to 2 mm of mercury. Then the unit was back-filled with argon to a pressure of about 2.5 psig. The system was periodically purged to get rid of contaminants.

c. Property determination

The tensile strengths, elastic moduli, and Poisson's ratios were determined from longitudinal and transverse specimens in both as-received condition and after thermal cycling. These tests were made with an Instron testing machine having a 10,000 pound capacity.

Aluminum grip tabs (0.5 x 1.5 inch) were glued to each end of the specimens with an epoxy adhesive to prevent premature failure of the test pieces in the jaws of the test machine. The specimen gage length was, therefore, 3 inches.

Half of the test pieces were instrumented with strain gages for the measurement of elastic moduli and Poisson's ratios. The response of these gages was monitored as a continuous trace on the strip chart of the test machine. Figure (4) shows an instrumented test specimen mounted in the tensile machine.

Boron fibers were extracted from cycled and uncycled specimens of each material type by dissolving away the matrix in a sodium hydroxide solution. Fifty fibers from each specimen were pulled in the testing machine and the failure loads recorded. Based on these loads and the measured fiber diameters, a statistical analysis was performed with the computer to determine the mean strength of each fiber set and the parameters of the Weibull statistical distribution to which the fiber strengths conform. From the Weibull parameters the mean of the distribution and the coefficient of variation were computed. The effects of the thermal cycling on the fiber strength could be evaluated from these results.

The composite density was also measured before and after cycling to ascertain if internal void formation occurred during cycling. These measurements were made by the Archimedes method which consists of weighing the sample first in air and then submerged in a liquid of known specific gravity. The liquid used was methyl ethyl ketone (MEK) which thoroughly wet the material. The analytical balance used to make the measurements could be read to an accuracy of 0.001 gram. The density was calculated using the formula

$$\rho = \frac{A\rho_{MEK}}{A+H-F}$$

where

A = weight of sample in air,

H = weight of sample holder in liquid,

F = weight of sample holder and sample in liquid,

ρ_{MEK} = density of MEK = 0.802 gm/cm.^{3}

2. Composite Expansion Measurements

a. Test specimens

Expansion curves of 1100, 2024, and 6061 Al-B were measured during 3, 6 and 12 minute thermal cycles. The specimens were approximately 6 x 0.5 x 0.04 inches. The 1100 and 2024 matrix materials were cut from the same panels used in the inert cycling tests. The 6061 matrix material contained about 45 v/o of 5.8 mil diameter fibers.

b. Apparatus

Figure (5) shows a photograph of the expansion measurement apparatus. A diagramatic representation is shown in Figure (6). The specimen was contained in a slot in a graphite block, the the bottom of which was mounted in a fixed support. One end of the specimen butted against the end of the slot while the other end was free to expand and move the armature of an LVDT via a graphite push-rod. During the heating half-cycle the furnace was lowered over the graphite block and removed during the cooling half-cycle. Air was blown around the block to provide cooling. A chromel-alumel thermocouple contacted the specimen to give the temperature throughout the cycle.

c. Test procedures.

The upper temperature limit measured at the mid point of the specimen was 425°c in all cases. The lower limit was about 45°c for a 12 minute cycle, 75°c for a 6 minute cycle and 160°c for a 3 minute cycle. A large temperature gradient existed along the length of the specimen, amounting to an almost 200°c difference between the two ends. The temperatues at each half inch along the specimen length was measured throughout each of the cycle periods.

In order to determine the actual composite specimen expansion it was necessary to know the expansion of the graphite holder at all times during the cycle. This was determined by measuring with the apparatus the response of a pure aluminum sample of known expansion characteristics. The expected aluminum expansion calculated from the expansion coefficients and known temperature

distribution was subtracted from the measured aluminum expansion response to find the expansive behavior of the graphite block and push rod. This graphite expansion was subtracted from each measured composite expansion curve to give the actual composite extension.

3. Low Temperature Cycling Tests

Nine specimens of 6061 aluminum reinforced with 5.8 mil diameter fibers were thermally cycled 3000 times between -100°c and +275°c. These limits were chosen to show the effects of both lower maximum temperatures and cyrogenic temperatures while keeping the cyclic temperature range the same as in prior cycling tests between ambient and 425°c. Three of the specimens were about 0.04 inch thick and contained 27 v/o fibers. Another set of three specimens were about 0.045 inch thick and contained 45 v/o fibers while the last three specimens were about 0.08 inch thick and contained about 45 v/o fibers. Thus, the effects of varying both the fiber volume fraction and the specimen thickness were studied.

Figure (7) shows a sketch of the low temperature cycling apparatus. It consisted of an asbestos box which contained two sets of resistance heating elements positioned in vertical planes on each side of the specimen plane. The specimens, each 6 x 0.5 inch, were stacked width-wise in the specimen plane and were separated from the heater elements by 0.125 inch thick graphite plates. The specimens were heated automatically during each cycle.

Cooling was provided by spraying liquid nitrogen vapor over the specimens during the cooling half cycle. Ambient temperature air was also blown over the heating coils and the graphite plates to cool them. A chromel-alumel thermocouple that could be positioned at the midpoint of any of the specimens was used to monitor the cyclic temperatures.

4. Superimposed Load Tests

Boron-6061 Aluminum composite specimens were cycled between room temperature and 365°c and between room temperature and 425°c while under load. Originally, an existing furnace previously constructed for thermal cycling unloaded composites in an air environment was modified to perform this experiment. Beam loading, see Figure (8), with a ratio of 6 to 1 was used. Universal joints were used at each end of the loading system to assure proper alignment. It was necessary to water cool the grips which held the specimen in order to prevent the grip section from flattening out and slipping out of the grips. Figure (9) shows a specimen in the grips.

Problems with boiler scale build-up in the grips, weld corrosion and consequent water leaks prompted a redesign of the system which would make water cooling of the grips unnecessary. The furnace in this case is much smaller than before and moves horizontally rather than vertically. Only the gage section of the specimen is heated and the grips remain cool. Cycling tests have not yet been completed using this arrangement.

III. Experimental Results

1. Inert Cycling Tests

a. Mechanical properties and density.

The measured ultimate tensile strengths, elastic moduli, and Poisson's ratios of the as-received and cycled 6061, 2024, and 1100 matrix boron-aluminum materials are compared in Tables 1, 2, and 3.

In Table 1 it may be seen that the strengths of the 6061 aluminum 4-mil boron longitudinal specimens thermally cycled in argon did not decrease below that of the as-received material. A 65% decrease in strength, however, was noted for those cycled in air. For the 6061 transverse specimens cycled in argon, a 9% decline in strength was measured using a 6 minute cycle and 23% using a 12 minute cycle. No transverse 6061 Al-B specimens were thermally cycled in air as part of this investigation. But results of other work at The University of Tennessee Space Institute indicate an average 31% decline in the transverse strength after 6000 cycles at 12 minutes/cycle.

The strength of 2024 aluminum reinforced with 5.8 mil boron fibers was also unchanged when cycled at either 6 or 12 minute periods, as seen in Table 2. But when they were cycled in air at 12 minutes/cycle, a 61% decrease was found. A large decrease in transverse strength during argon gas thermal cycling was measured for the 2024 material. Part of this decrease may be attributable to annealing of the matrix rather than degradation. A 5% greater

strength loss was measured for the 12 minutes/cycle in air than for those in argon.

Similarly to the other materials, the 1100 matrix results, tabulated in Table 3, show little or no longitudinal strength degradation in argon, but a 44% decrease in air. The transverse strength dropped from 8 ksi in the as-received condition to 6 ksi for both 6 and 12 minutes/cycle in the inert gas to 4 ksi at 12 minutes/cycle in air.

In comparing the three types of material it is seen that the 2024 was the strongest as-received and the 6061 was the weakest. The 6061 matrix material also showed the greatest longitudinal strength degradation in air. The least strength loss was evidenced by the 1100 material.

Due to the amount of scatter in the modulus and Poisson's ratio data, it is not possible to determine from them any trends in the behavior of these properties when subjected to the various thermal cycling treatments.

The results of the fiber strength tests described in the previous section are summarized in Table 4. The arithmetic, geometric, and Weibull mean strengths are given for each set of fibers. Also shown are the Weibull parameters, ω and σ_o, and the coefficient of variation, a measure of data scatter. The last column gives the percent change in Weibull mean fiber strength compared to as-received.

Little change in strength was obtained for the fibers extracted from argon atmosphere cycled specimens with the exception of the 2024 Al-B at 12 minutes/cycle. A 9% decrease from the as-received strength level was found for those fibers.

Quite large fiber strength degradations, on the other hand, were measured for those extracted from specimens thermally cycled in air. The decreases were 48, 23, and 18%, respectively, for the 6061, 2024, and 1100 matrix materials.

Also, as indicated in Table 4, the variation in fiber strength for the 2024 and 6061 matrix composites increased during air cycling compared to that measured for as-received fibers, the greatest change being in the 2024 material. A smaller increase in strength variation occurred for those fibers cycled in argon at 12 minutes/cycle. The least change is seen in the 1100 material fiber scatter.

The change in composite density resulting from thermal cycling in argon or air is shown in Table 5. Despite the data scatter it is evident that an appreciably larger density change occurred during cycling in air than occurred in the argon environment. This indicates the formation of more internal voids in air cycled materials. It may be seen that the largest apparent density change was in the 1100 material. The reason for this is not clear.

b. Metallographic observations

Observations of the fracture surfaces of longitudinal composite specimens revealed some information about the failure modes and the quality of the interfacial bond. No significant changes in the macroscopic fracture appearances were evident due to thermal cycling in either environment. The 6061 matrix specimens containing 4-mil fibers displayed a slightly jagged fracture surface, indicating a somewhat ductile failure. This was probably caused by deviation from perfect bonding, as evidenced by a significant amount of fiber pullout. The 2024 material, however, showed a relatively flat fracture and no fiber pullout, indicative of good consolidation and bonding. The 1100 matrix material exhibited an extremely jagged fracture appearance with large amounts of fiber pullout.

Observation of the specimens' surface appearance before and after thermal cycling provided an indication of the amount of degradation. As viewed through a low power microscope, all of the cycled specimens displayed a greater amount of surface roughness than did the uncycled ones. However, the extent of this roughness was considerably greater for those cycled in air. The greatest difference was evident for the 2024 matrix composite and the least for the 1100 material. Little surface cracking was found for the argon cycled specimens, but a great deal for the air cycled ones.

The results of two studies using a scanning electron microscope proved inconclusive. The first consisted of examining the aluminum matrix fracture appearance to detect differences that might be correlated with the amount of matrix degradation. It was suspected that the more damaged ones would show a more open, honeycomb-type fracture appearance due to the presence of reaction products. However, from the limited number of samples examined, it could not be determined that such was the case.

The purpose of the second SEM study was to compare the relative amounts of reaction product on extracted boron fibers. If fiber oxidation occurred in air, then more reaction material would be expected on the air cycled fibers. No conclusive trend, however, was apparent. Due to the non-uniform distribution of the reaction products, it was concluded that quite a large number of fibers would have to be examined to positively determine correlations between visible fiber degradation and thermal cycling conditions or measured strength.

2. Expansion Measurements

Plots of the expansion behavior of 1100, 2024, and 6061 aluminum-boron during thermal cycling are shown in Figure (10), (11), and (12) respectively. From these curves it is apparent that there is some change in the expansion of the composite due to changing the matrix alloy. In addition, changing the cycle period produces a marked change in the deformation, the shortest cycle period producing the greatest amount of composite extension.

3. Low Temperature Cycling Tests

The room temperature tensile strengths of specimens cycled to low temperatures are shown in Table 6. All of the strengths are within the strength ranges of the as-received materials. Therefore, no decrease in strength was found when B-Al was thermally cycled between -100°c and 275°c. Figures (13), (14), and (15) are photographs of the surface appearances of the three types of specimens before cycling and after 3000 cycles. Significant surface roughening but very little cracking was observed. The 27 v/o material showed the greatest degree of roughening, presumedly because of the thicker Al surface layers.

4. Superimposed Load Tests

From the data, Table 7 , we can see that there is no measurable strength decrease caused by cycling between room temperature and 365°c using any of the applied stresses. There was a strength decrease observed in specimens cycled between room temperature and 425°c. These strengths, however, are within the range of those cycled with no applied load. Thus, the initial indication is that these small applied tensile stresses do not affect the rate of thermal degradation. Since the strength of the composite is reduced as the number of thermal cycles increases it is reasoned that larger applied stresses will eventually cause the specimen to fail before 6000 thermal cycles have been applied.

5. Carbon-Aluminum Cycling Tests

The results of these tests can be seen in Tables 8 and 9. Table 8 contains results obtained from three 0.75 x 0.09 inch specimens. These specimens were cycled between room temperature and 425°c using a 3 minute period. The flexual modulus decreased after cycling while the tensile modulus did not. This decrease can be misleading since the formula used to determine the flexual modulus is very dependent on specimen thickness and these specimens show large dimensional changes due to cycling (see Table 10).

Table 9 contains results obtained from specimens cut from a panel of 0.72 inch thick carbon-2024 aluminum. This panel had very low transverse properties before cycling. Transverse specimens could not withstand an appreciable number of thermal cycles for they fell apart after only 500 thermal cycles, see Figure (16). The specimens cycled to 425°c suffered a large longitudinal strength decrease. The higher temperature specimens exhibited a surface roughening and cracking that was even more severe than that associated with the surface of specimens of boron-aluminum. This can be seen in Figure (17) where surface cracks large enough for the fibers to be seen were developed.

At this time, it is believed that the mechanism of thermal cycling degradation is similar to that in boron-aluminum. At the present time additional specimens are being cycled in argon.

IV. Discussion

1. Theoretical Evaluation of Thermal Cycling Stresses and Strains

In metal matrix composites having appreciably different thermal expansion coefficients between the component phases, large internal stresses may be generated due to changes in temperature. Such stresses are generated during the service life of composites subjected to varying temperatures and are the driving forces behind such damage mechanisms as thermal fatigue, corrosion fatigue, and creep.

Residual stresses are produced in cooling from fabrication temperatures, as reported by Ebert and Wright [7]. It is reasoned that the material is originally stress free at the fabrication temperature of approximately 500°c for B-Al. As the temperature is decreased, the large longitudinal contraction of the matrix is constrained by the fibers. This results in the generation of longitudinal tensile stresses in the matrix and balancing compressive stresses in the fibers.

In order to evaluate the actual stresses and strains that are to be expected due to a change in temperature, an analysis is required which includes both time independent plastic deformation and time dependent plastic flow, that is, creep. Creep effects would be expected to be very significant in an aluminum matrix subjected to high temperature and high stress.

The stress equilibrium condition is given by the rule of mixtures as

$$\sigma_f v_f + \sigma_m v_m = \sigma_c = \sigma_a \tag{1}$$

where σ_f, σ_m and σ_c are the stresses on the fibers, matrix and composite respectively and v_f and v_m are the component volume fractions. The strain conformity relation is

$$\int_{T_1}^{T_2} \alpha_m dT + \varepsilon_m = \int_{T_1}^{T_2} \alpha_f \, dT + \varepsilon_f \tag{2}$$

where α_m and α_f are the component linear expansion coefficients and ε is the mechanical strain produced in one component by the restaint of the other. The total mechanical strain of either component of the composite is given by

$$\varepsilon = \varepsilon_e + \varepsilon_p + \varepsilon_c \tag{3}$$

where

ε_e = elastic strain

ε_p= time independent plastic strain,

ε_c= creep strain

Considering a one-dimensional state of stress and strain, ε_e is given for either phase by

$$\varepsilon_e = \frac{\sigma}{E} \tag{4}$$

Since the fibers may be assumed to always remain elastic, then

$$\varepsilon_f = (\varepsilon_e)_f \tag{5}$$

The matrix plastic strain term may be provided by the commonly accepted relationship that exists between stress and strain after yielding

$$\sigma_m = \sigma_o + K\,[(\varepsilon_m)_p]^n$$

where

σ_o = yield stress,

K_*, n = constants.

Solving for the strain,

$$(\varepsilon_m)p = \pm\left[\frac{(\sigma_m-\sigma_o)}{k*}\right]^{1/n} \qquad (6)$$

The Dorn equation is employed for steady-state creep:

$$\varepsilon_c = A\left(\frac{|\sigma_m|}{G}\right)^s \frac{Gb}{kt}\, D_o\, e^{-Q/RT}$$

where

G = shear modulus,

Q = creep activation energy,

b = Burger's vector,

k = Boltzmann's constant,

R = gas constant,

A,S, D_o = constants.

Integrating over the temperature range of interest:

$$(\varepsilon_m)_c = \int_{T_1}^{T_2} (\varepsilon_m)_c \left(\frac{dt}{dT}\right)\, dT$$

$$= \int_{T_1}^{T_2} A\left(\frac{|\sigma_m|}{G}\right)^s \frac{Gb}{kT}\, D_o\, e^{-Q/RT} \left(\frac{dt}{dT}\right) dT \qquad (7)$$

By summing these strain components, substituting into Eq. (2) and eliminating σ_f by the use of Eq. (1), a single equation is obtained for the matrix stress, σ_m, as

$$\int_{T_1}^{T_2} (\alpha_m - \alpha_f)\, dT = \frac{\sigma_a - \sigma_m V_m}{V_f E_f} - \{\frac{\sigma_m}{E_m} \pm [\frac{\sigma_m - \sigma_o}{K_*}]^{1/n} \pm \int_{T_1}^{T_2} A(\frac{|\sigma_m|}{G})^s \frac{Gb}{kT} D_o e^{-Q/RT} (\frac{dt}{dT})\, dT\} \tag{8}$$

where σ_a is the applied stress and $\frac{dt}{dT}$ is the inverse of the heating rate.

This equation may be solved by numerical methods and a computer program was written for this purpose. The matrix stress, σ_m, was evaluated for an assumed constant rate of cooling from the 500 °c fabrication temperature to room temperature and subsequently, for a number of thermal cycles. The temperature values used during the cycles were those measured at the midpoints of specimens in the thermal expansion experiments. From the calculated matrix stress, the fiber stress and strain and the matrix strain components were also obtained by the use of Eqs. (1), (4), (6), and (7).

Values for the temperature dependent properties, α_m, E_m, σ_o, G, and Q, were obtained by linearly interpolating between tabulated values. The fiber properties, α_f and E_f, were assumed to be temperature independent. Values used for the constants K_* ,

n,A,s, and D_o are

$K_* = 1.0 \times 10^5$ psi,

$n = 0.5$,

$s = 4.4$,

$A = 3.3942 \times 10^6/°K$,

$D_o = 0.2651 \frac{in^2}{sec}$.

The 2024 alloy was used for the matrix in these calculations because of the availability of property data. Two cycle rates, 6 and 12 minutes/cycle, were evaluated in order to determine the effect of frequency. The constant cooling rate from fabrication temperature was somewhat arbitrarily chosen to be 1°c per second.

The calculated matrix stress versus temperature for a 12 minute cycle is shown in Figure (18). It may be seen that only two cycles are required to produce a steady hysteresis loop. As the temperature decreases from the fabrication temperature of 500°c the matrix is constrained by the fibers, and a tensile stress is generated in it. The matrix stress increases slowly at first because of stress relief by creep. But by about 100°c the rate of stress relaxation is greatly reduced and the stress rises sharply, exceeding the yield point of the matrix. As the temperature rises again during the subsequent thermal cycles, the tensile stress decreases rapidly as the matrix expands. Now, a compressive stress is generated in the matrix which reaches a peak at 150°c. At this point creep becomes sufficient to provide stress relief so that the matrix stress decreases toward zero as the temperature continues to increase. The cooling rate from a

maximum cyclic temperature of 425°c is slow enough that creep prevents the matrix stress from again exceeding the yield point. The cyclic stress limits are shown to be 11 ksi tensile and 5 ksi compressive, a stress range of 16 ksi.

The stress-strain curve exhibited by the matrix is indicated in Figure (19). Upon heating from the lower cyclic temperature limit, the curve initially decreases linearly, indicating elastic strain. After the compressive peak, creep reduces the stress until it again approaches zero. The strain rate is initially rapid on cooling due to creep. But at about 100°c, it decreases with decreased creep until the low temperature limit is again reached. Figure (20) shows the creep strain as a function of temperature. As the temperature increases from near room temperature the tensile creep strain in the matrix is unchanged until 150°c is reached; that is, negligible creep occurs. After 150°c the creep strain decreases at a constant rate of 24 inch/inch per °c to a minimun at the upper temperature. The fiber stresses as a function of temperature are shown in Figure (21). They are slightly higher than the matrix stresses because a 45 v/o of fibers was used.

The curves for the 6 minutes/cycle stresses and strains, Figures (22) and (23), are seen to be almost identical to those of 12 minutes/cycle, except that the maximum tensile stress and strain are less because of a higher minimum temperature. The reason for this would seem to be that the calculated creep strain is dominated by temperature rather than time.

The results indicate that little or no gross plastic deformation of the matrix occurs during cycling between room

temperature and 425 °c. It therefore appears that the large amounts of cyclic creep strain that occur are responsible for the surface ratcheting and matrix cracking that is observed.

2. Comparison of Theoretical and Measured Composite Expansions

It may be seen that the curves in Figures (10), (11), and (12) for the 3 minute/cycle expansions are negative near the minimum temperature. That is, the length of the composite is shown to be smaller at about 160°c than at room temperature, an obvious impossibility. The expansion curves during cooling at 6 minutes/cycle also seem to be low. Comparison of the maximum expansion at 6 minutes/cycle with that calculated using the equation

$$\left(\frac{\Delta L}{L}\right)_c = \alpha_f \Delta T + \varepsilon_f \qquad (9)$$

see Figure (24), would seem to indicate that the measured maximum expansion is too large. The hysteresis in the measured curve is also considerably greater than that in the calculated one. The reason for all of these apparent inaccuracies is not known at the present time but is being investigated.

3. Thermal Cycling Damage Mechanisms

a) Matrix Degradation. Thermal cycling of aluminum matrix composites in air produces surface roughening and cracking as shown in Figure (25). For boron-aluminum, significant roughening occurs after approximately a thousand or so thermal cycles using maximum cycle temperatures above about 400°c. The extent of roughening increases with increasing number of cycles until visible cracks are evident. The cracks usually appear to start at the valleys between surface layer fibers. Later, transverse cracks develop from valley to valley across the fiber ridges. This process is depicted in the sketch of Figure (26). After a larger number of cycles, the matrix surface material inside areas outlined by the cracks tends to ball-up or form nodules as seen in Figure (27). Sometimes fibers are exposed between these nodules.

The extent of surface roughening and cracking appears to be even greater for graphite-aluminum than for boron-aluminum under the same thermal cycling conditions, Figs. (28) and (17). At least this was the case for the two lots of material tested thus far. The reasons for this have not yet been established. The surface damage consists of wrinkle-like surface roughening leading to extensive cracking transverse to the fiber axis. These cracks expose the underlying fibers. Since the aluminum surface layers provided most of the strength of transverse specimens, once they become extensively cracked, the specimens fall apart. Another characteristic of the thermal cycling damage produced in C-al is the large dimensional changes that are observed. These may be related to the large radial expansion of the graphite fibers [6].

The factors that lead to increased thermal cycling damage seems to be the same for both B-Al and C-Al. These are 1) increased maximum temperature above some critical minimum, 2) increased temperature range, 3) increased cyclic period, 4) increased matrix alloying, and 5) exposure to an active environment. The first three of these result in increased matrix cyclic strain while the last two decrease the ability of the matrix to tolerate these strains. As for the fibers, the first three factors increase the reactivity of the fibers with the matrix and the environment and the last two provide exposure to the enviornment. In cycling between room temperature and 425°c, the creep strains appear to be dominant. In cycling between -100°c and 275°c, both plastic deformation and creep deformation are expected. However, inspection of equation (5) indicates that the total cyclic matrix strain expected is probably less than that expected for similar specimens cycled between room temperature and 425°c. Thus, a smaller amount of roughening and cracking is observed.

The results of tests in which boron-aluminum was cycled while also sustaining an applied load, thus far indicate that matrix degradation, and in fact composite degradation, is independent of applied tensile stress. This is really to be expected since the matrix carries very little tensile load.

Thermal expansion measurements made as the boron-aluminum material was cycled indicate that the longitudinal displacement, and hence the matrix stress, varies with the length of the cyclic period but is practically independent of the matrix alloy, ie, matrix strength. The largest displacements and therefore largest stresses exist for the shortest cycle periods. This is contrary to the extent of composite degradation

which is a maximum at the longest cycle periods. It is apparent, therefore, that the degradation does not occur as a result of stress fatigue. Rather, it is a result of matrix plastic strain fatigue acting in conjunction, apparently, with some environmentally related mechanisms. In cycling between room temperature and elevated temperatures such as 425 °c, cyclic creep appears to constitute most of the plastic strain.

Based upon the data in Tables 1, 2, and 3, matrix degradation is believed to be facilitated by some environmentally related mechanisms such as oxidation embrittlement, corrosion fatigue or hydrogen embrittlement.

Corrosion fatigue is defined as the reduction of fatigue resistance due to the presence of a corrosive medium [9] . While the exact mechanisms of corrosion fatigue in aluminum and its alloys are as yet uncertain, the phenomenological aspects are quite well known. The principal ones are listed here [10, 11, 12, 13].

1. Water vapor is the primary agent affecting the fatigue properties. Depending upon the alloy and various test variables, moisture can increase the rate of crack growth by a factor of ten or more. Dry oxygen and hydrogen have only a small effect at room temperature. The effect on pure Al is somewhat greater than on its alloys. Dry nitrogen and argon have essentially no effect. The effect of humid gases is predominantly determined by their water vapor content.

2. The fatigue crack growth rate varies with water vapor pressure. The rate is essentially unaffected until a threshold pressure is reached and then, usually within one order of magnitude change, increases rapidly with increasing pressure. This threshold or transition pressure has been found to increase with both increasing frequency and crack length.

3. An increase in test frequency results in a larger number of cycles to failure because of the lesser amount of time for environmental interactions. At high stress intensity levels the actual time to failure is usually less. However, at low amplitudes, it is often longer due to increased endurance limit.

4. The magnitude of the enviornmental effect is greatest at low values of the stress intensity amplitude, K, corresponding to the shortest crack lengths. At high values of K approaching K_c, the environmental sensitivity decreases due to the predominanting gross plasticity effects.

5. Thin sections are less environmentally sensitive. Wei [10] ascribes this to the increased stress-relieving effect of plastic deformation associated with a transition from a plane stress to a plane strain mode of fracture. According to the hydrogen embrittlement mechanism, the environmentally produced stresses are believed to be generated by the pressure of hydrogen evolved in the matrix.

6. At a given K level, the fatigue crack growth rate increases with increasing temperature.

7. Distinct failure striations are produced in air but not in vacuum. Aggressive environments at low frequencies and amplitudes result in a change from normal ductile striations to brittle striations. These are flat, reflective facets exhibiting faint crack arrest markings.

The numerous mechanisms proposed by investigators to explain corrosion fatigue crack growth in aluminum may be grouped broadly into three classes: (1) gas adsorption, (2) hydrogen embrittlement, and (3) slip interaction with surface oxide films. The first model considers that gas molecules adhering to crack faces prevent crack rewelding and reversed slip when the crack closes up during unloading or compression [14] The second model proposes that atomic hydrogen produced by water vapor reacting with aluminum diffuses into the region ahead of the crack, super-saturating the lattice and reducing its strength. Subsequent precipitation of molecular hydrogen may produce voids ahead of the crack tip which would coalesce during the next tensile half-cycle [10] . The third mechanism, sometimes called the "wet film model" states that wet oxide surface films attract dislocations, resulting in slip band and crack formation, while dry oxide films do not [15].

Smith and Shahanian [16] have demonstrated the effect of water vapor in the air on the room temperature fatigue life of B-Al composites in bending. Transverse specimens flexed in the thickness direction showed an appreciable decrease in fatigue life when the test was carried out in a 2 torr water vapor environment.

Longitudinal specimens cycled in water vapor in the thickness direction showed a factor of 90 increase in crack growth rate compared to vacuum. While it is not sure how results from this type of test would relate to those under cyclic tension, it is evident that a large effect of moisture exists, possibly even greater than that of the aluminum alone.

Another environmentally controlled process leading to increased thermal cycling damage is matrix oxidation. A surface film of aluminum oxide is formed on the matrix even at room temperature. This film may be produced by reaction of the aluminum with atomspheric oxygen or by reaction with water vapor, particularly at elevated temperatures. Normally, this oxide film serves as a barrier against further surface reaction. However, if the cyclic thermal and creep strains are able to break up the protective film and expose fresh aluminum surfaces to the air, then reaction will proceed and possibly produce nucleation sites for the formation of fatigue cracks.

Aluminum oxide films may also cause matrix surface disruption by a process called spheroidization [17]. The high surface tension of the oxide film tends to cause the surface material to ball-up at high temperatures when the aluminum is extremely soft. An example of matrix surface spheroidization is shown in Figure (27).

The observed effects of temperature, cyclic frequency, and alloy type correlate well with the corrosion fatigue mechanism. Since corrosion fatigue is dependent upon both temperature and time, the greatest damage would be expected at high temperature and

low cycle frequency, as is observed. Alloying is believed to increase the extent of corrosion fatigue by such mechanisms as galvanic effects, increased internal energy, and creep interference leading to higher stresses.

Water vapor in the air is most likely the principal environmental agent in thermal corrosion fatigue of the matrix, as it has been shown to be in mechanical corrosion fatigue of aluminum.

b) Interface and Fiber Degradation

The loss of strength by B-Al composites subjected to thermal cycling has generally been attributed either to the growth of an aluminum-diboride reaction zone at or next to the interface or to fiber oxidation once they are exposed to the air by matrix cracking. Figure (29) shows an extracted boron fiber covered with reaction products. According to the explanation, based on the formation of AlB_2 , the highly nonuniform character of the reaction products is supposed to introduce stress concentrations which lower the fiber fracture strengths. This idea was supported by experiments by Metcalfe [17] which showed that if the AlB_2 reaction layer was removed from the fibers, then their strengths would return to near their original values.

The results of the present investigation show that if air is excluded from the environment, then the strengths of boron fibers and the B-Al composite are essentially unaffected by thermal cycling. Among the possibilities as to why the fibers are more degraded in the presence of air are:

1) severe matrix damage in air (corrosion fatigue, etc.) causing mechanical breakup of both the interface and the AlB_2 reaction layer producing stress concentrations,

2) increased AlB_2 reaction in presence of air,

3) different AlB_2 geometry in air, ie. more jagged, nonuniform reaction products and higher stress concentrations,

4) oxidation of the fibers; ie, formation of boron oxide.

Which of these really occur could only be determined by experiment. Additional investigation is needed to determine the constitution of the interface and interphase reaction zone after various thermal cycling treatments. Comparison of the amounts and topography of these reaction products is needed.

The general conclusion based on all thermal cycling experiments done at the University of Tennessee Space Institute is that increased fiber degradation correlates with increasing matrix degradation. While it is probable that the increased fiber damage occurs as a result of matrix deterioration, this has not yet been proven.

V. Conclusions

1. Boron-aluminum composites thermally cycled to a maximum temperature of 425° c for 6000 cycles exhibited large longitudinal and transverse strength degradations in air but not in argon.

2. Boron fibers extracted from specimens thermally cycled in argon showed little or no strength decrease while those from air cycled specimens showed decreases as high as almost 50%.

3. Cycling in air produced a greater amount of surface roughening and cracking than did cycling in argon.

4. The greatest amount of B-Al matrix damage was indicated by the 2024 meterial, a moderate amount by the 6061, and the least by the 1100 material.

5. The greatest strength degradation of B-Al composite and fibers was for the 6061 material. The 1100 material showed the least strength degradation.

6. Density measurements indicated more void formation in B-Al specimens thermally cycled in air than in argon.

7. Increased B-Al matrix degradation in air was attributed to corrosion fatigue due to the presence of water vapor in the air.

8. Lower boron fiber strengths and consequent composite strengths were believed to result from either fiber oxidation or more extensive interfacial layer breakup.

9. Thermal cycling damage to boron-aluminum composites and probably other aluminum matrix composites in the temperature range of ambient to 425°c can be greatly reduced or practically eliminated by preventing contact with the atmosphere. With this protection such composites may be used without significant degradation at much higher temperatures, perhaps 500°c or higher, than is otherwise possible.

10. Applied tensile stresses do not appear to affect the thermal cycling behavior of boron-aluminum composites.

11. B-Al composites subjected to 3000 cycles in air between -100°c and +275°c showed significant surface roughening but no reduction in tensile strength.

12. Expansion measurements of B-Al during thermal cycling, though incomplete, indicate that the displacement is greatly dependent upon cyclic period but practically independent of matrix alloy.

13. Theoretical calculations of B-Al composite stresses and strains during thermal cycling between ambient and 425°c show that little or no time independent plastic deformation but large amounts of cyclic creep deformation occur. These results, together with those of the expansion measurements, indicate that the cyclic creep strains along with environmental effects, are the cause of the observed matrix roughening and cracking in air.

14. Graphite-aluminum composites subjected to 6000 thermal cycles at 3 minutes/cycle between ambient and 425°c showed a large but misleading decrease in flexual modulus, no change in the tensile modulus, and tensile strength reductions as high as

about 70%. Transverse specimens began falling apart after about 500 cycles. The extent of surface roughening and cracking was even greater than that for boron-aluminum. Longitudinal specimens cycled between ambient and 365°c showed no strength decrease.

REFERENCES

1. Wright, M.A., and B. Intwala, "The Effect of Elevated Temperatures on the Mechanical Properties of B-Al Composites," Journal of Material Science, Part VIII, 7:957-963, July 1973.

2. Dardi, L.E., and K.G. Kreider, "Effect of Soft Water and High Temperature Exposure on Boron-Aluminum Composites," Composite Materials: Testing and Design (Third Conference) ASTM STP 546, 1974, pp. 269-283.

3. Shahansan, P. "Thermal Fatigue of Boron-Aluminum Composites," SAMPE Quarterly, 2128-35, June, 1970.

4. Wright, M.A., "The Effects of Elevated TEmperatures on the Structural Properties of Fiber Composite Materials Suitable for Use in Space Shuttle and Other Space Vehicles." NASA Contract No. UT844001-6463R-95, Final Report, University of Tenn. Space Institute, October, 1972.

5. Wright, M.A., "The Mechanical Properties of Metal Matrix Composites Subjected to Cyclic Temperature Changes." Technical Report prepared under Navy Contract No. N00014-71-A-0121-0003 NR 031-760 by the University of Tennessee Space Institute, October, 1974.

6. Harrigan, William C. Jr., "The Effects of Thermal Cycling on the Strengths of Aluminum-Graphite Composites," Technical Report, Aerospace Corporation, July, 1974.

7. Ebert, L.J., and P.K. Wright, "Mechanical Aspects of the Interface," Composite Materials-Volume 1, Interfaces in Metal Matrix Composites. A.G. Metcalfe, editor, New York: Academic Press, Inc., 1974, pp. 31-64.

8. Garmong, G. "Elastic-Plastic Analysis of Deformation Induced by Thermal Stress in Eutectic Composites," Metallurgical Transactions, 5: 2183-2205, October, 1974.

9. Fontane, F.G., and N.D. Green, Corrosion Engineering, New York: McGraw-Hill Book Company, Inc. 1967.

10. Wei, R.P. "Some Aspects of Environmental Enhanced Fatigue-Crack Growth," Journal of Engineering Fracture Mechanics, 1: 633-651, 1970.

11. Hockenhull, B.S., H.A. Monks, and H. Sala, "Frequency and Environmental Interactions in the Fatigue of Aluminum Alloys," Corrosion Fatigue: Chemistry, Mechanics and Microstructure, NACE, 1972, pp. 453-458.

12. Krupp, W.E., D.W. Hoepporen, and E.K. Walker, "Crack Propagation of Aluminum Alloys in Corrosive Environments," Corrosion Fatigue: Chemistry, Mechanics and Microstructure, NACE, 1972, pp. 468-483.

13. Freeney, J.A., J.C. McMillan, and R.P. Wei, "Environmental Fatigue Crack Propagation of Aluminum Alloys at Low Stress Intensity Levels," Metallurgical Transactions, 1, 1741-1757, June 1970.

14. Wadsworth, N.J., and J. Hutchings, "The Effect of Atmospheric Corrosion and Metal Fatigue," Philosophical Magazine, 3: 1154-1166, 1955.

15. Enochs, J.S., and O.F. Devereaux, "Fatigue Crack Growth in 5052-H34 Aluminum in Vacuum and Active Gas Environments" Metallurgical Transactions, 6A: 391-397, February, 1975.

16. Smith, H.H., and P. Shananian, "Effect of Water Vapor on Fatigue Behavior of an Aluminum-Boron Composite," Corrosion Fatigue: Chemistry, Mechanics and Microstructure. NACE, 1972, pp. 499-505.

17. Metcalfe, A.G., "Physical Chemical Aspects of the Interface," Composite Materials- Vol. 1, Interfaces in Metal Matrix Composites, A.G. Metcalf, editor, 1974, pp. 31-64.

Table 1

Measured Mechanical Properties of 6061 Matrix B-Al Composite

Matrix	Orientation	Cycle Period (min.)	Atm.	UTS[a] (ksi)	ΔUTS (%)	$E_{11}x10^{-6}$ (psi)	$E_{22}x10^{-6}$ (psi)	ν_{21}	ν_{12}
6061	Long.	AR	-	171.0	-	40.3	-	0.242	-
		6	Inert	175.6	+2.7	33.3	-	0.230	-
		12	Inert	184.4	+7.8	34.3	-	0.250	-
		12	Air	59.9	-65.0	32.7[a]	-	0.221	-
6061	Trans.	AR	-	16.4	-	-	17.9	-	0.100
		6	Inert	15.0	-8.5	-	17.9	-	0.118
		12	Inert	12.6	-23.2	-	15.0	-	0.106
		12	Air	11.3[b]	-31.1	-	15.2	-	0.154

[a]Average of two specimens.

[b][30].

Table 2

Measured Mechanical Properties of 2024 Matrix B-Al Composite

Matrix	Orientation	Cycle Period (min.)	Atm.	UTS (ksi)	ΔUTS (%)	$E_{11}x10^{-6}$ (psi)	$E_{22}x10^{-6}$ (psi)	ν_{21}	ν_{12}
2024	Long.	AR	-	206.0[a]	-	36.4	-	0.250	-
	Long.	6	Inert	209.9[a]	+1.9	32.1	-	0.237	-
	Long.	12	Inert	210.0[a]	+1.9	31.6	-	0.250	-
	Long.	12	Air	80.3[a]	-61.0	38.8[a]	-	0.243	-
2024	Trans.	AR	-	38.0[a]	-	-	19.6	-	0.099
	Trans.	6	Inert	14.4[a]	-62.1	-	21.0	-	0.129
	Trans.	12	Inert	10.7[a]	-71.8	-	9.4[a]	-	0.105
	Trans.	12	Air	8.6	-77.4	-	16.5	-	0.104

[a]Average of two specimens.

Table 3

Measured Mechanical Properties of 1100 Matrix B-Al Composite

Matrix	Orientation	Cycle Period (min.)	Atm.	UTS (ksi)	ΔUTS (%)	$E_{11} \times 10^{-6}$ (psi)	$E_{22} \times 10^{-6}$ (psi)	ν_{21}	ν_{12}
1100	Long.	AR	-	192.1[a]	-	33.8	-	0.247	-
	Long.	6	Inert	186.5[a]	-2.9	30.9	-	0.236	-
	Long.	12	Inert	196.1[a]	+2.1	30.5	-	0.238	-
	Long.	12	Air	108.4[a]	-43.6	30.5[a]	-	0.233	-
1100	Trans.	AR	-	8.1[a]	-	-	17.5	-	0.147
	Trans.	6	Inert	6.1[a]	-24.7	-	12.9	-	0.103
	Trans.	12	Inert	6.0[a]	-25.9	-	12.7[a]	-	0.057
	Trans.	12	Air	4.3	-46.9	-	11.1	-	

[a]Average of two specimens.

Table 4

Experimental Data for Extracted 2 Inch Long Boron Fibers

Matrix	Period (min.)	Atm.	$\bar{\sigma}_A$ (ksi)	$\bar{\sigma}_G$ (ksi)	$\bar{\sigma}_W$ (ksi)	ω	σ_o (ksi)	Coeff. of Variation	$(\Delta\bar{\sigma}_W)$ %
6061[a]	AR[b]	-	432.8	412.4	424.4	9.943	832	0.121	-
	6	Argon	434.4	424.5	427.4	11.292	773	0.107	+0.7
	12	Argon	421.6	371.4	413.9	7.573	992	0.156	-2.5
	12	Air	231.3	213.4	222.8	6.254	640	0.187	-47.5
2024[c]	AR	-	514.0	490.8	505.9	13.231	818	0.092	-
	6	Argon	503.8	491.5	495.1	14.846	760	0.083	-2.2
	12	Argon	471.6	436.6	459.8	11.509	799	0.105	-9.1
	12	Air	363.8	345.4	388.9	2.763	361	0.391	-23.1
1100[c]	AR	-	436.0	372.8	428.0	6.219	1,180	0.188	-
	6	Argon	436.7	424.6	426.7	8.587	891	0.139	-0.3
	12	Argon	438.2	427.8	426.8	7.743	964	0.153	-0.3
	12	Air	361.7	344.0	352.2	8.748	725	0.137	-17.7

[a] 4.0 mil diameter fibers.

[b] AR = As received.

[c] 5.8 mil diameter fibers.

Table 5

Density Measurements of As-Received and Thermally Cycled B-Al

Matrix	Orien-tation	Cycle Period (min.)	Atmosphere	Density (gm/cm^3)	Δ Density (%)
6061	Long.	AR	-	2.6411	-
6061	Long.	6	Inert	2.6333	-0.30
6061	Long.	12	Inert	2.6540	+0.49
6061	Long.	12	Air	2.5627	-2.97
6061	Trans.	AR	-	2.6198	-
6061	Trans.	6	Inert	2.6376	+0.68
6061	Trans.	12	Inert	2.6272	+0.28
2024	Long.	AR	-	2.6380	-
2024	Long.	6	Inert	2.6266	-0.43
2024	Long.	12	Inert	2.6304	-0.29
2024	Long.	12	Air	2.5974	-1.54
2024	Trans.	AR	-	2.6253	-
2024	Trans.	6	Inert	2.6075	-0.68
2024	Trans.	12	Inert	2.6168	-0.32
2024	Trans.	12	Air	2.5808	-1.72
1100	Long.	AR	-	2.5944	-
1100	Long.	6	Inert	2.5367	-2.22
1100	Long.	12	Inert	2.5830	-0.44
1100	Long.	12	Air	2.4463	-5.71
1100	Trans.	AR	-	2.6039	-
1100	Trans.	6	Inert	2.5970	-0.46
1100	Trans.	12	Inert	2.5538	-1.96
1100	Trans.	12	Air	2.4600	-5.53

Table 6

6061 Al-B Thermally Cycled Between - 100°C and +275°C

Spec.	No. of Cycles	Thickness	Percent Fibers	UTS (ksi)
1	2000	.040	27	83.3
2	3000	.040	27	123.2
3	3000	.040	27	96.7
1	2000	.045	45	226.9
2	3000	.045	45	217.4
3	3000	.045	45	212.4
1	3000	.080	45	242.1
2	3000	.080	45	198.2
3	3000	.080	45	212.1

TABLE 7

MEASURED MECHANICAL PROPERTIES OF 6061 MATRIX B-AL COMPOSITES CYCLED UNDER EXTERNAL LOADS

Specimen	Cycle	T max	Stress	UTS KSI	E MSI
1	3	365°c	15 KSI	215.2	---
2	3	365°c	30 KSI	193.13	31.84
3	3	365°c	50 KSI	202.64	31.94
4	6	425°c	15 KSI	125.8	32.5
5	6	425°c	30 KSI	95*	----

* Specimen failed in grips

TABLE 8
MEASURED MECHANICAL PROPERTIES OF CARBON-ALUMINUM COMPOSITES

Specimen #	E Tension Before Cycling MSI	E Tension After Cycling MSI	E Bending Before Cycling MSI	E Bending ** After Cycling MSI	σ uts Before Cycling KSI	σ uts After Cycling KSI
1	25.85	-----	17.9	----	78.87*	-----
2	-----	18.9	13.3	9.55	-----	38.92
3	-----	20.1	18.9	8.44	-----	47.25

NOTE: σ uts calculated using area before cycling

* Specimen failed in grips

** E in bending calculated using $E = \frac{P L^3}{y_{48} I}$ where $I = \frac{b h^3}{12}$

Note I strongly dependent on h and h used for after cycling was after cycling h.

See dimension changes. All cycling R. T. to 425° 3 min. cycle.

TABLE 9

MEASURED MECHANICAL PROPERTIES OF 2024 MATRIX C-Al COMPOSITES

Specimen #	Type	Cycle Temp.	E in MSI	σ uts in KSI
1	long	60 C- 425 C	21.74	25.174
2	long	60 C-425 C	19.4	21.94
3	trans	60 C-425 C	----	-----
4	trans	60 C-425 C	-----	-----
5	long	as-received	20.175	82.644 86.052
6	trans	as-received	1.18	1.737
7	long	60 C-365 C	20.55	88.6
8	long	60 C-365 C	-----	73.5

Specimen Failed in grips

No transverse specimens where pulled after cycling since none survived cycling.

Specimen failed in grips and was pulled again, failing in grips a second time.

TABLE 10

DIMENSION CHANGES IN C-A1 SPECIMENS DUE TO CYCLING

SPECIAL SPECIMEN #2

	Before Cycling		After Cycling	
	Width	Depth	Width	Depth
Top	.7499	.0867	.8076	.0968
Middle	.7493	.0873	.8288	.1023
Bottom	.7506	.0875	.8161	.1008
Average	.7499	.0872	.8175	.08997
	area = .06539"		area = .08173"	

2024 MATRIX SPECIMEN #1

	Before Cycling		After Cycling	
	Width	Depth	Width	Depth
Top	.5023	.0722	.5410	.0866
Middle	.5012	.0719	.6230	.0958
Bottom	.4997	.0717	.5576	.0892
Average	.5011	.0719	.57387	.0892
	area = .03603"		area = .05119"	

All cycling R.T. to 425°C 3 min. cycle

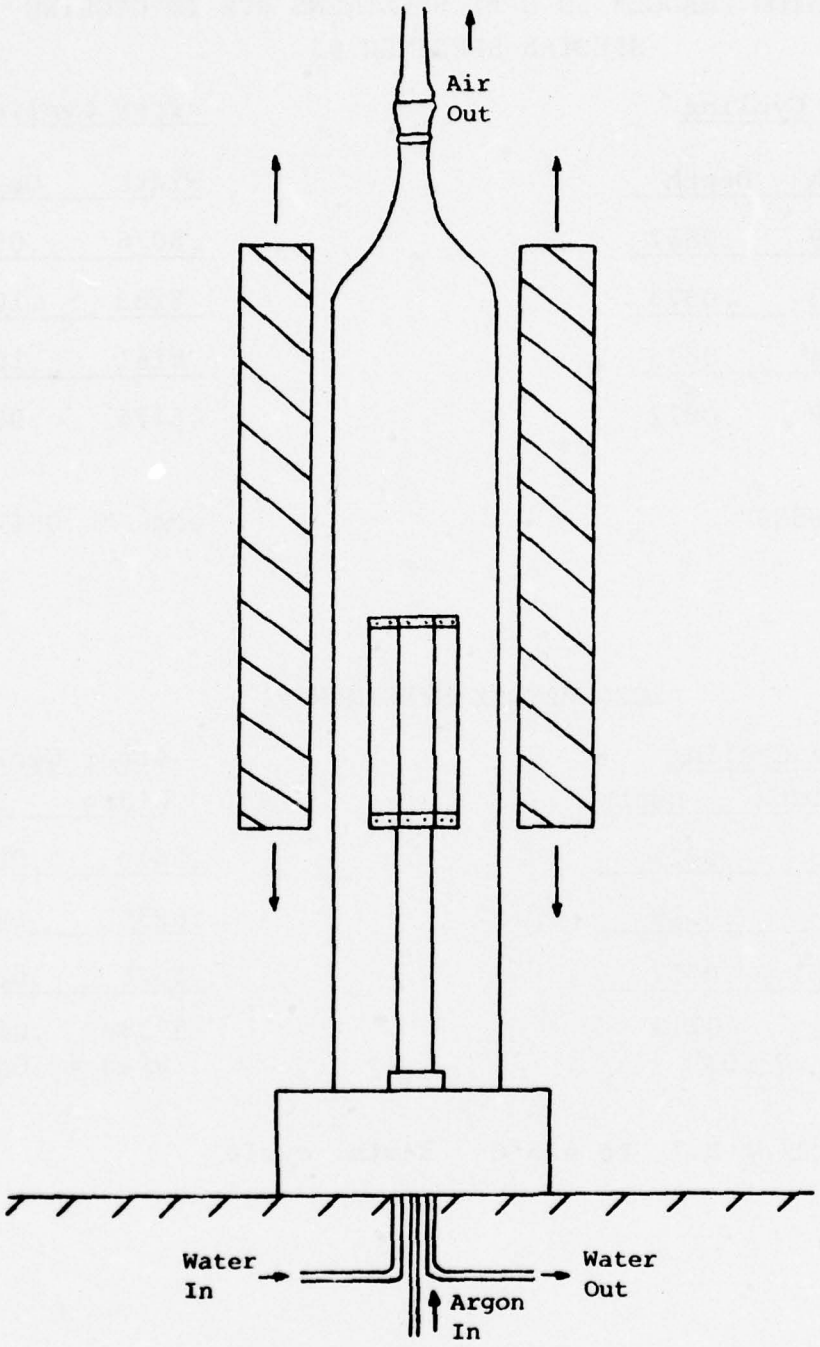

Figure 1. A diagram of the controlled atmosphere thermal cycling furnace.

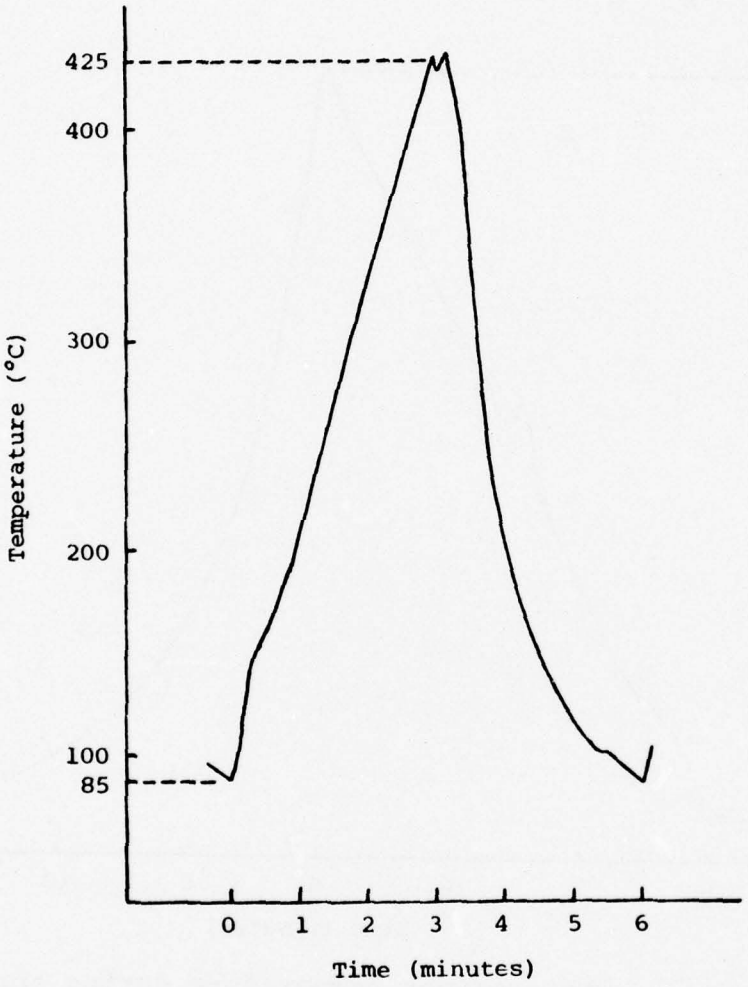

Figure 2. The specimen temperature during thermal cycling, 6 minutes/cycle.

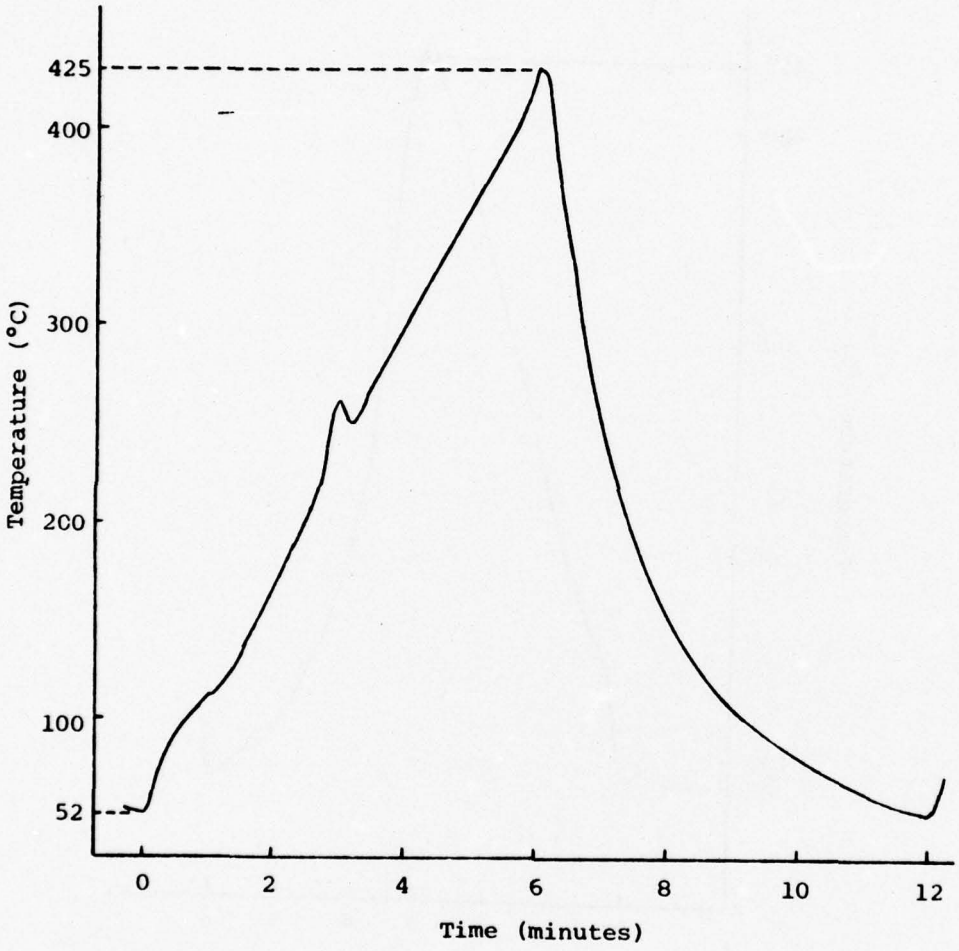

Figure 3. The specimen temperature during thermal cycling, 12 minutes/cycle.

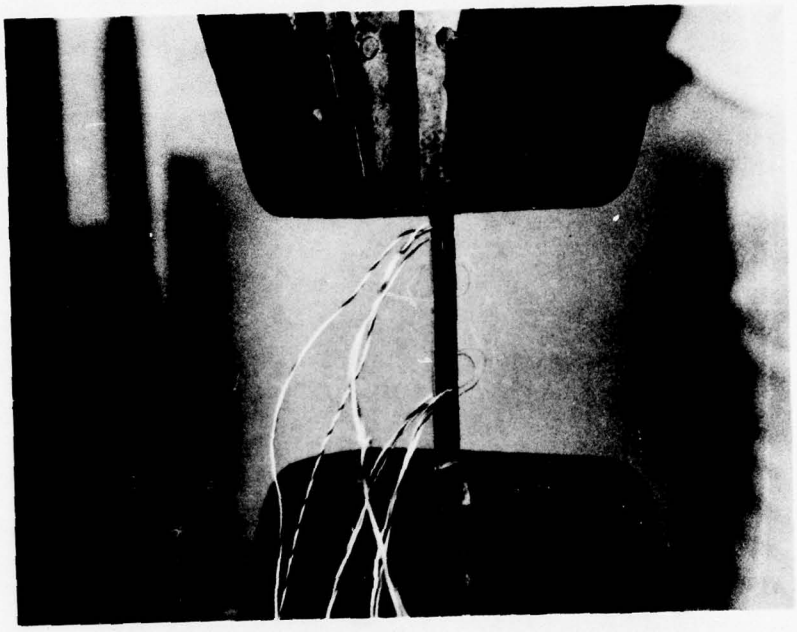

Figure 4. An instrumented composite specimen gripped in the tensile machine.

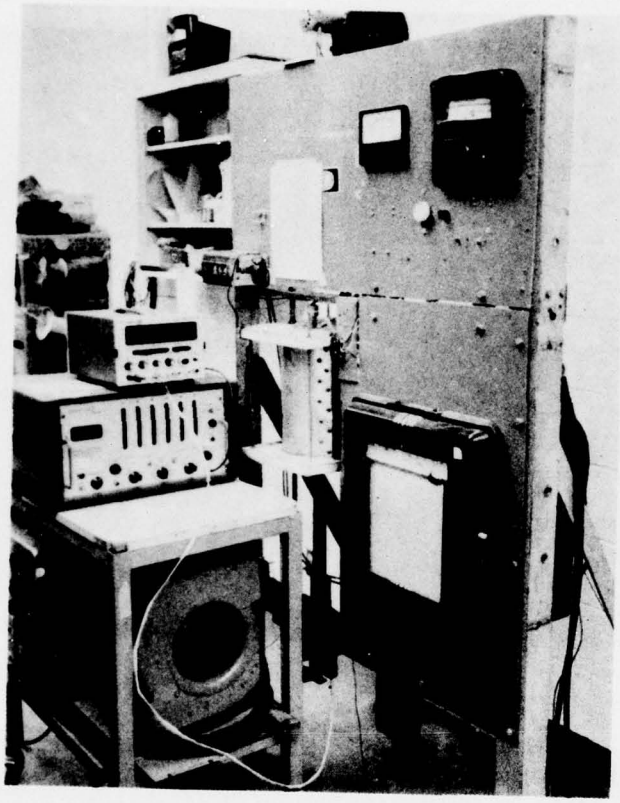

Figure 5. Apparatus for expansion measurement during thermal cycling.

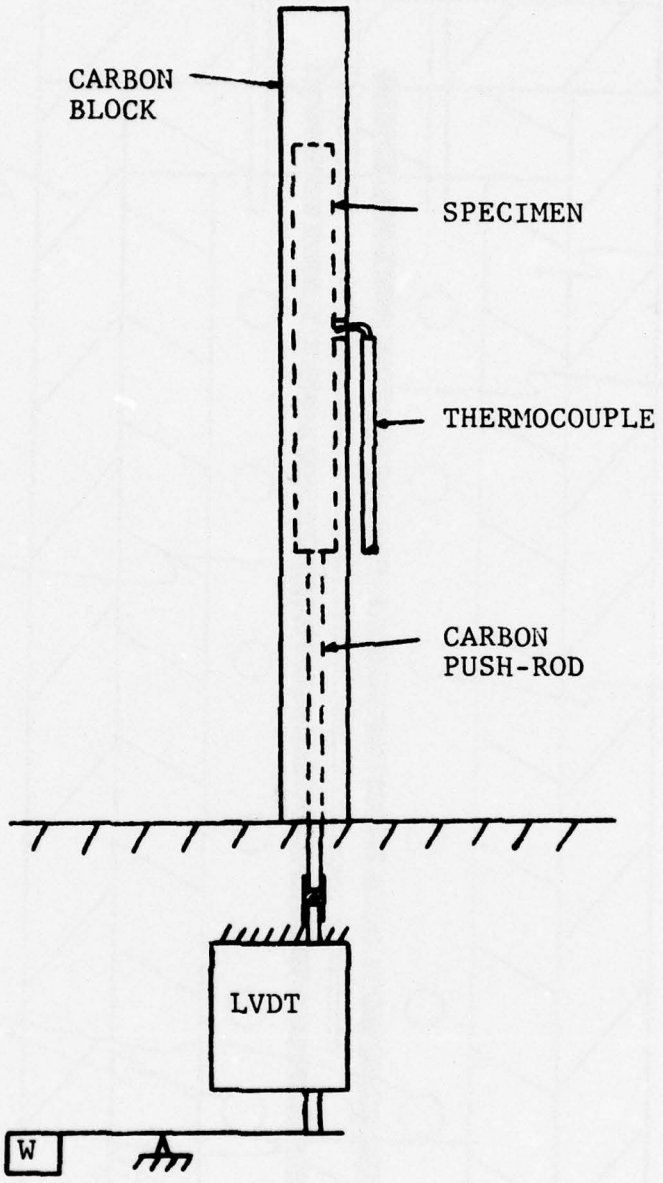

Figure 6. Diagram of the expansion measurement apparatus.

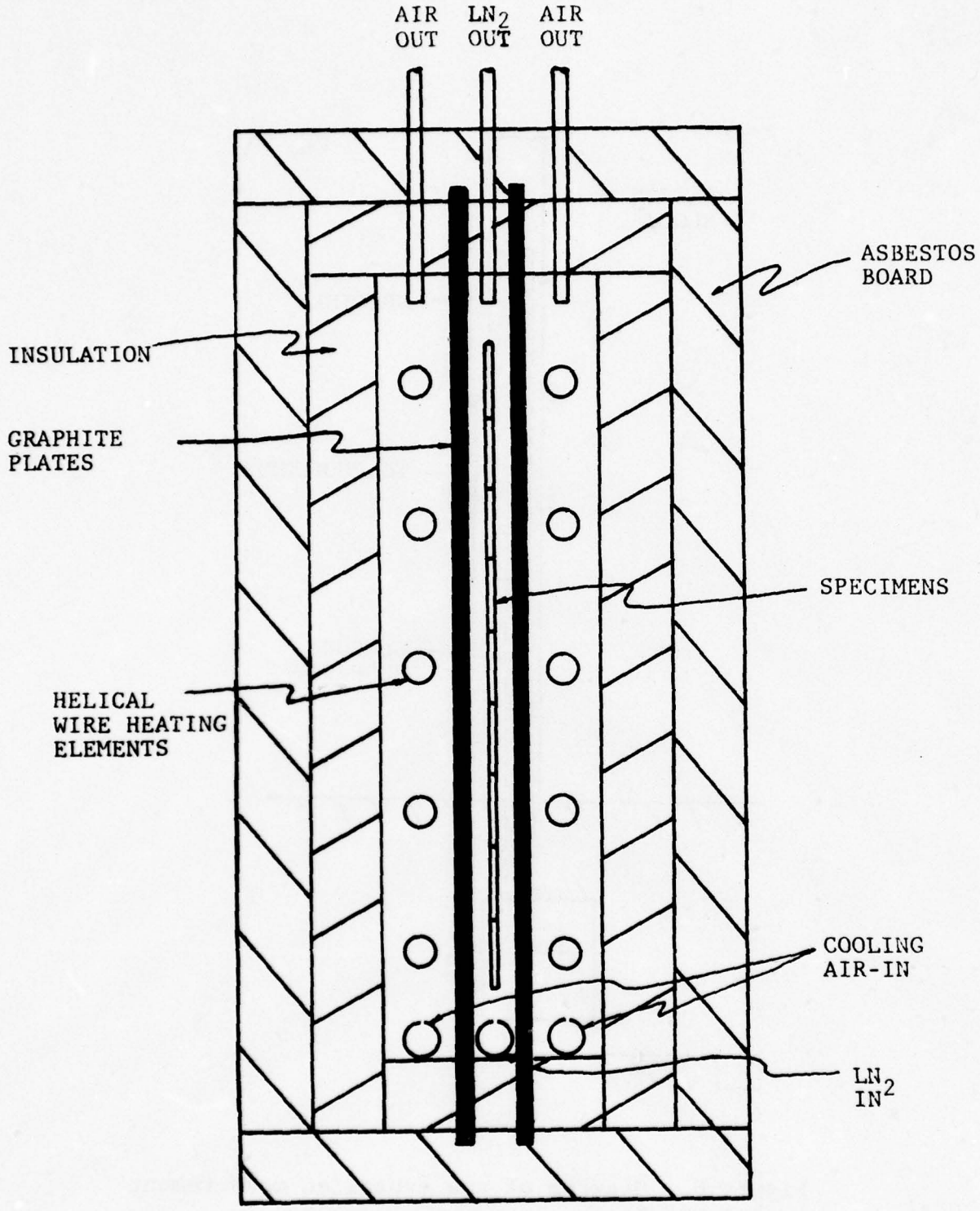

Figure 7. Diagram of the low temperature cycling apparatus.

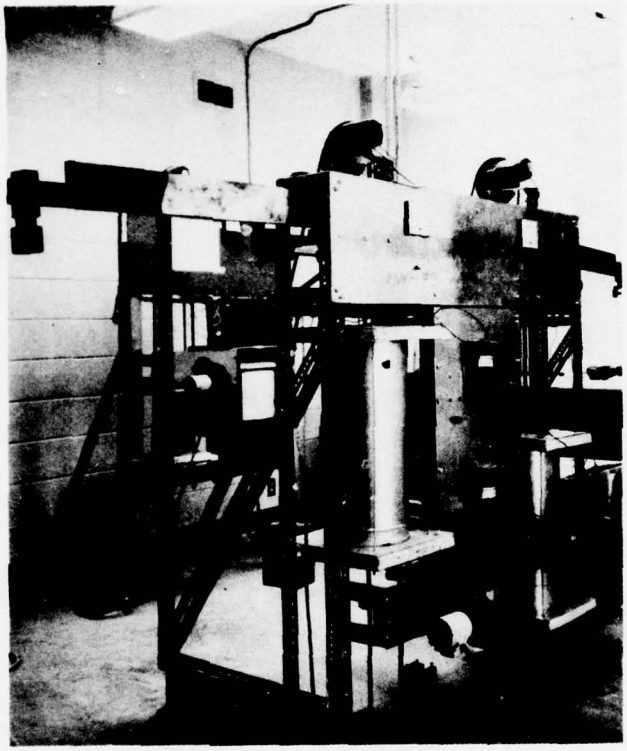

Figure 8. Furnace unit used for thermal cycling under static load.

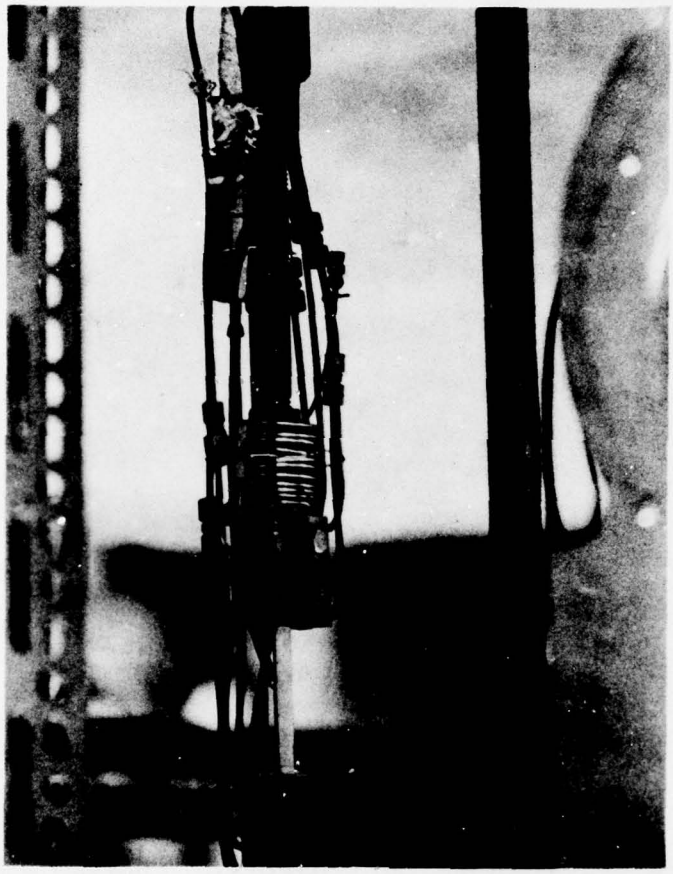

Figure 9. Water cooled grips used for thermal cycling under static load.

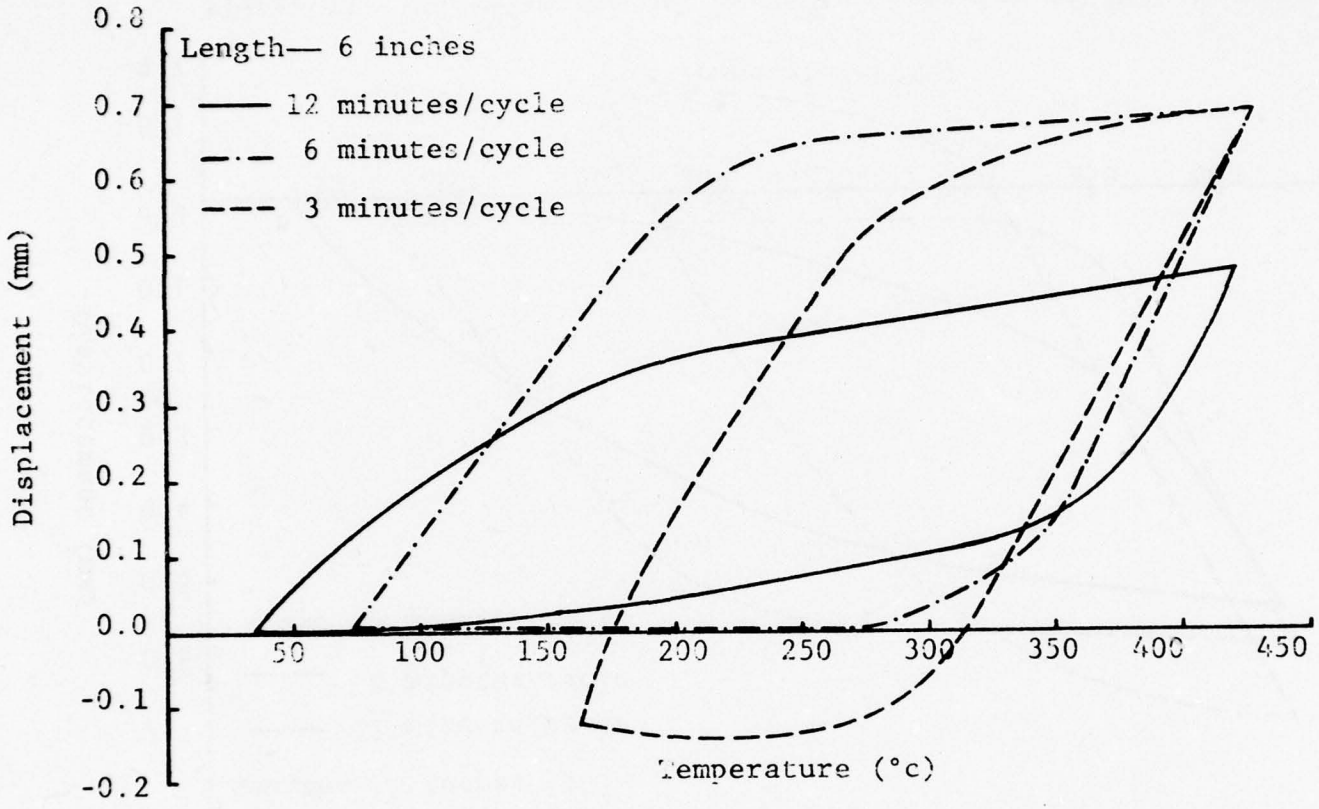

Figure 10. Measured thermal expansion behavior of 1100 aluminum-boron.

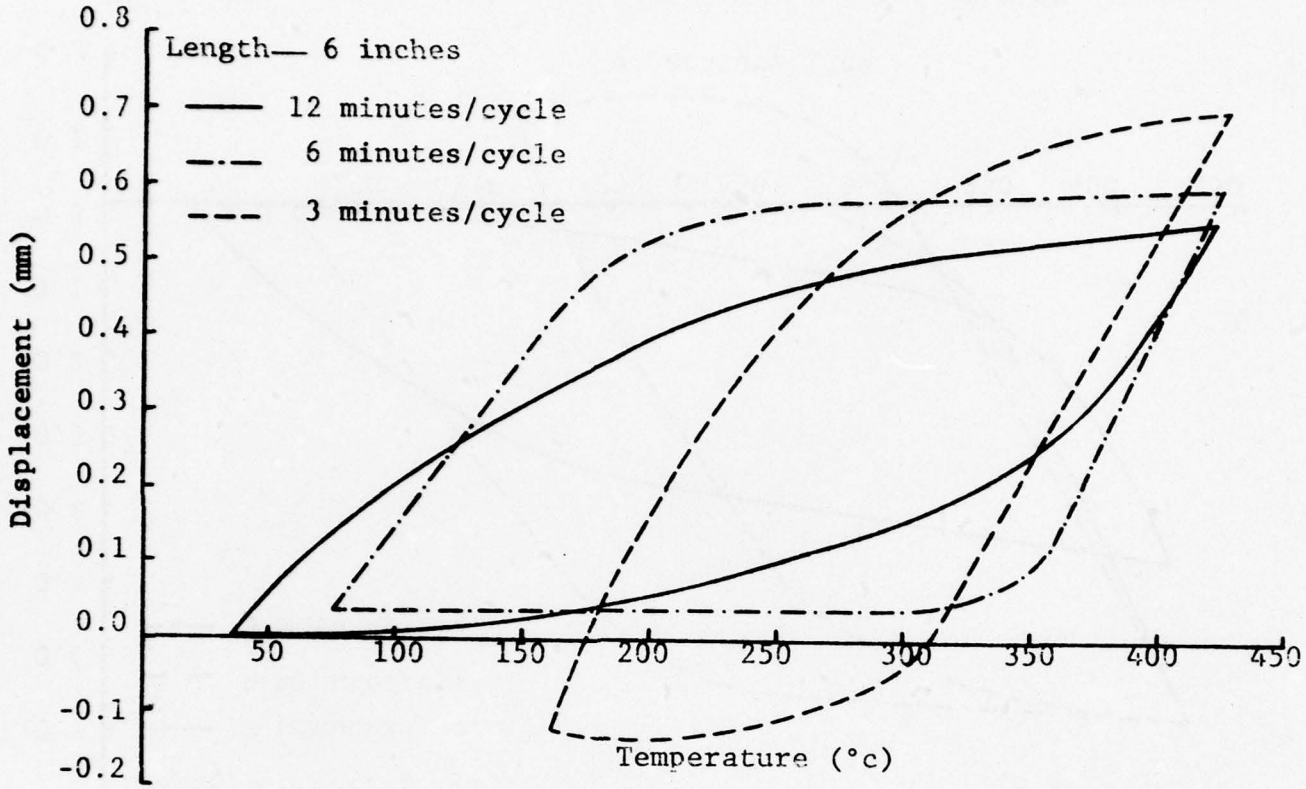

Figure 11. Measured thermal expansion behavior of 2024 aluminum-boron.

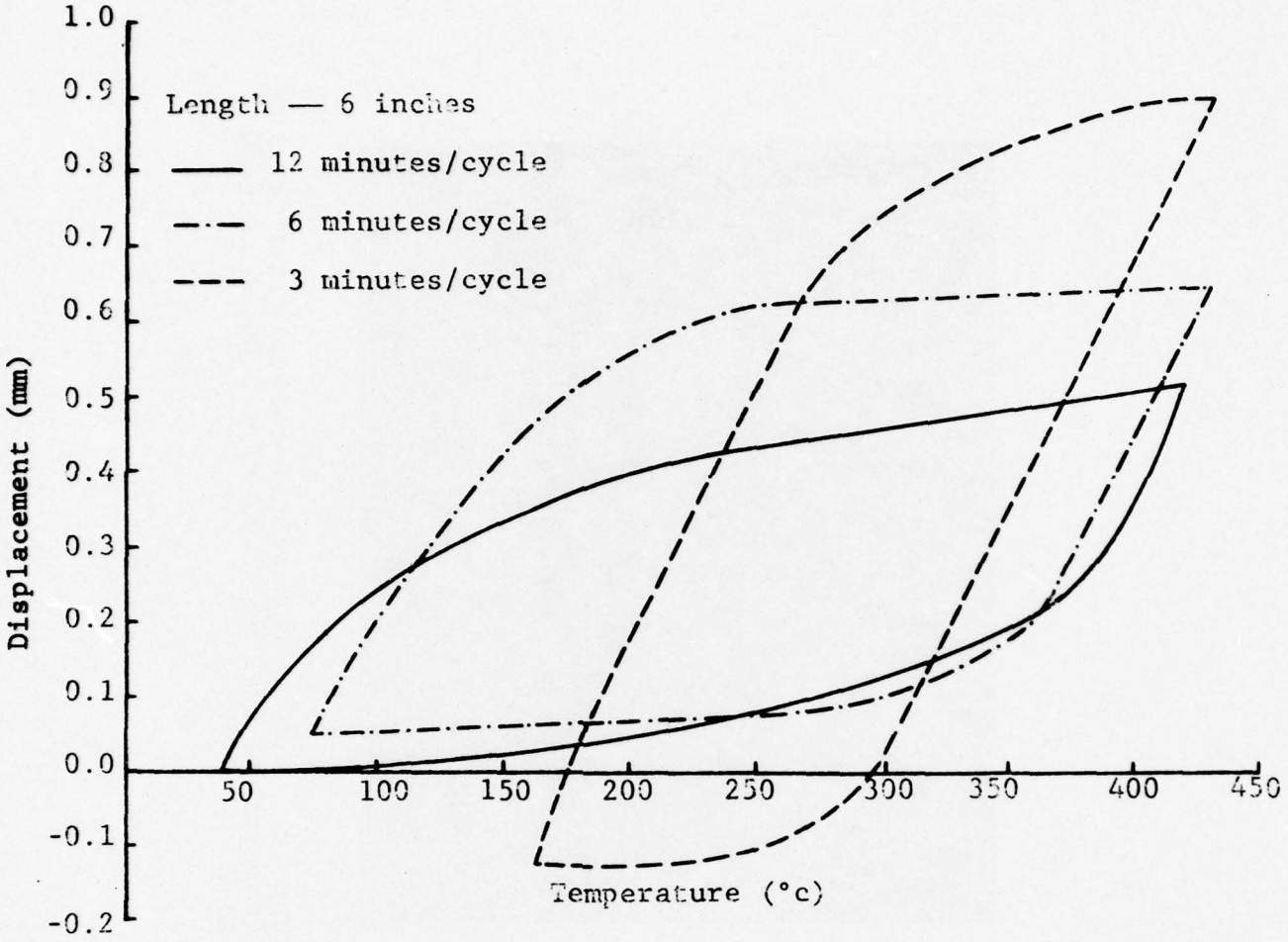

Figure 12. Measured thermal expansion behavior of 6061 aluminum-boron.

Figure 13. Surface appearance before and after low temperature cycling of 27 v/o, 0.04 thick 6061 Al-B.

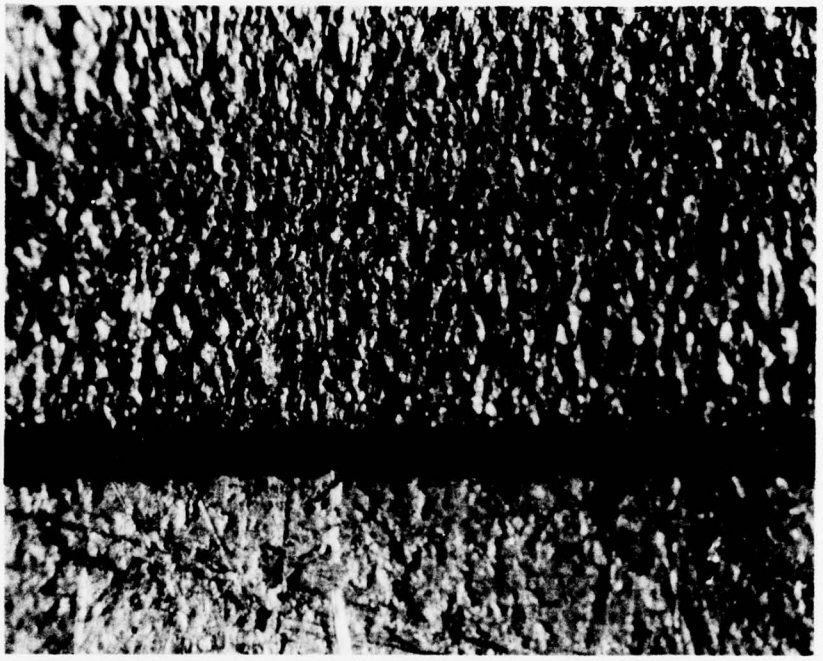

Figure 14. Surface appearance before and after low temperature cycling of 45 v/o, 0.045 thick 6061 Al-B.

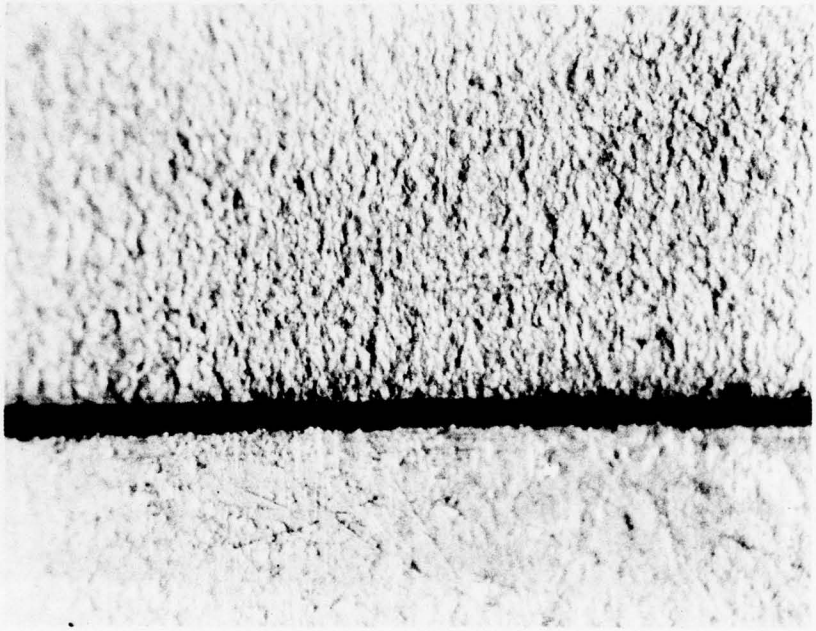

Figure 15. Surface appearance before and after low temperature cycling of 45 v/o, 0.08 thick 6061 Al-B.

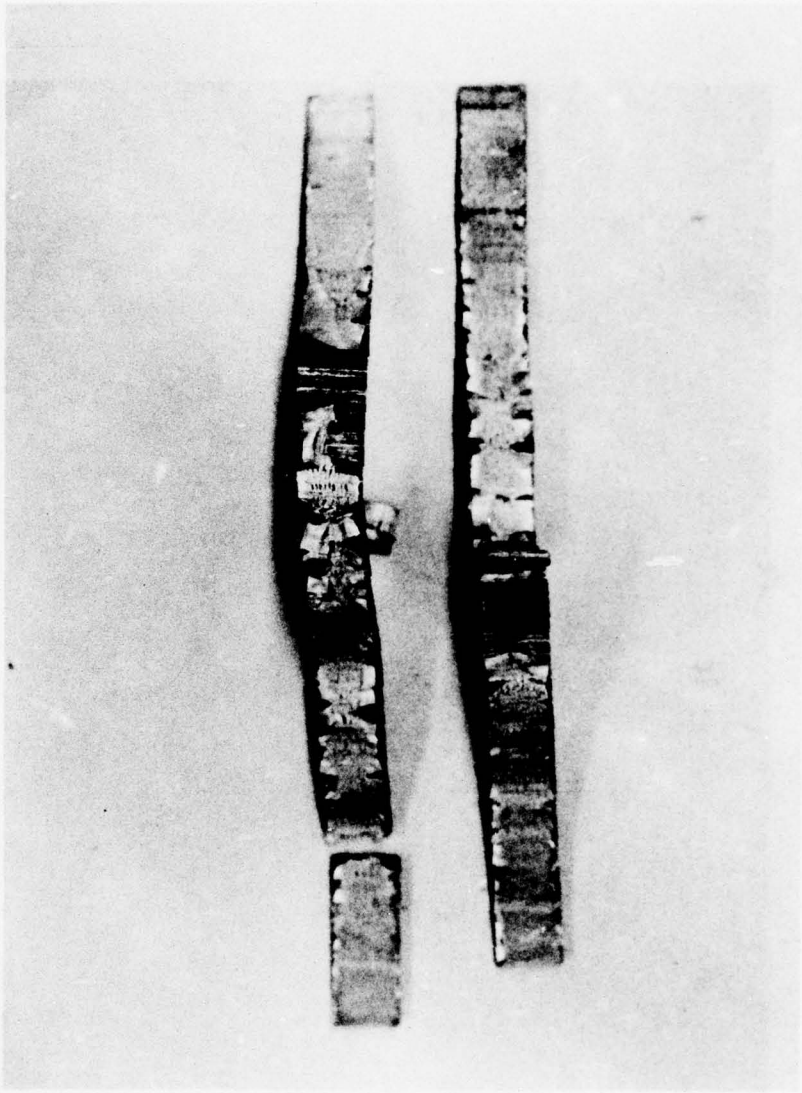

Figure 16. Thermally cycled transverse carbon-2024 aluminum specimens.

Figure 17. Crack in surface of thermally cycled longitudinal carbon-2024 aluminum at a magnification of 350.

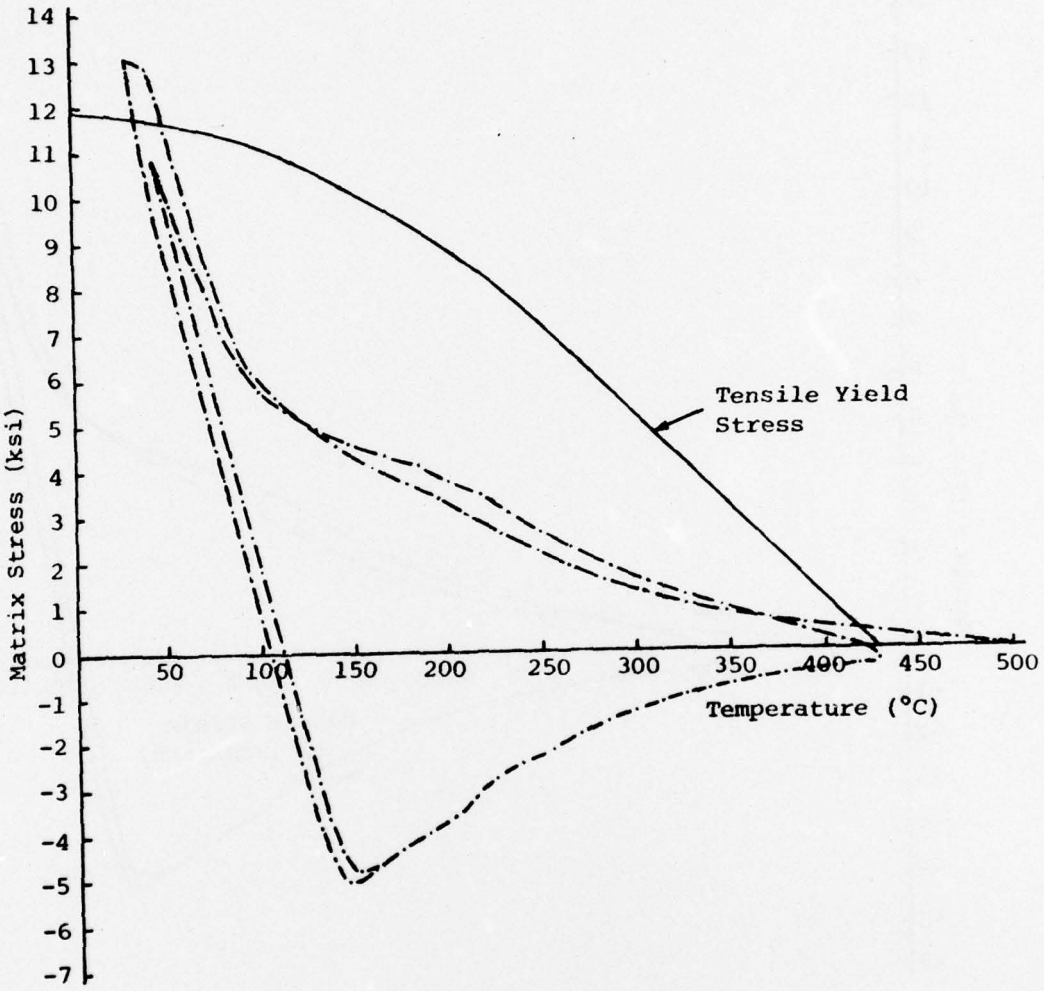

Figure 18. The matrix stress in thermally cycled 2024 aluminum-boron, 12 minutes/cycle.

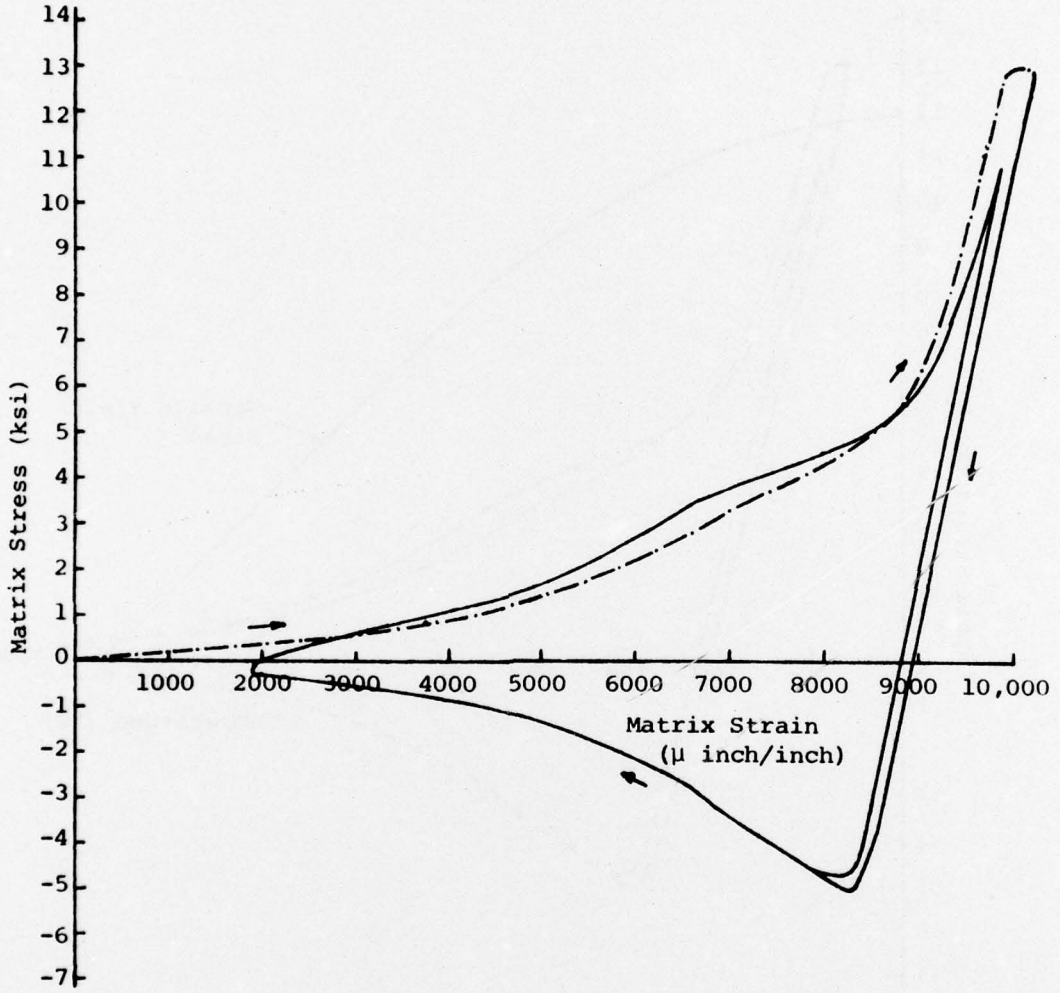

Figure 19. The matrix stress-strain curve during thermal cycling of 2024 aluminum-boron, 12 minutes/cycle.

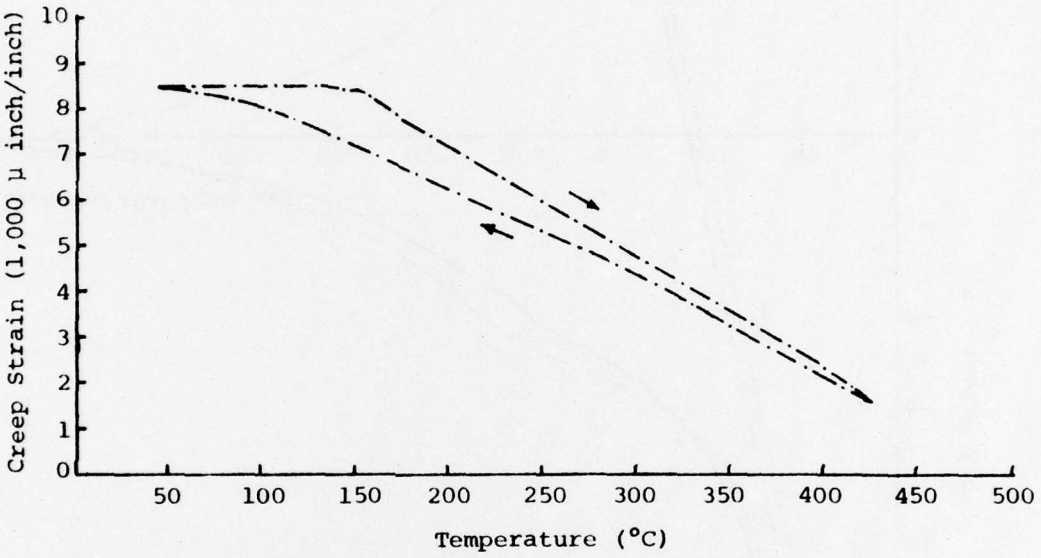

Figure 20. The creep strain during thermal cycling of 2024 aluminum-boron, 12 minutes/cycle.

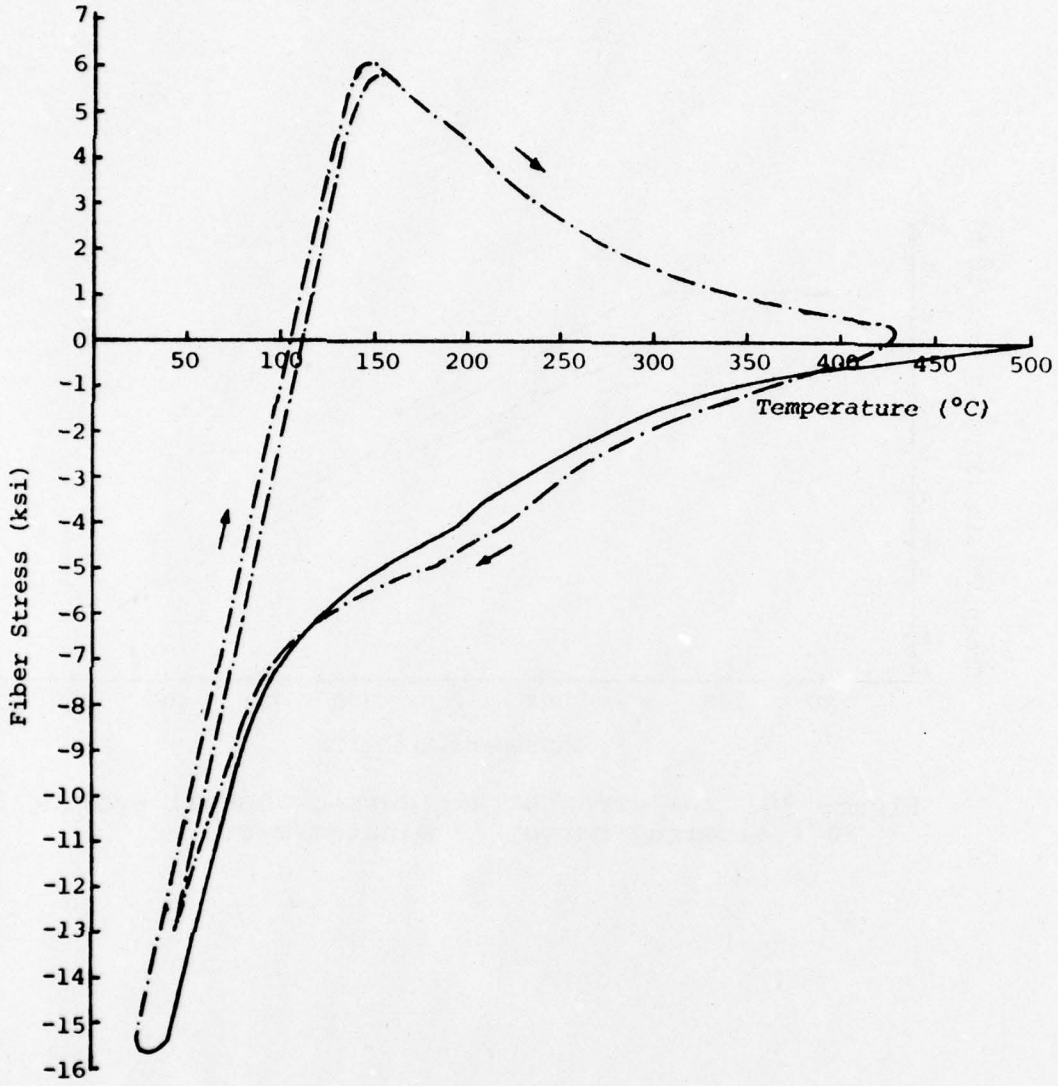

Figure 21. The fiber stress during thermal cycling of 2024 aluminum-boron, 12 minutes/cycle.

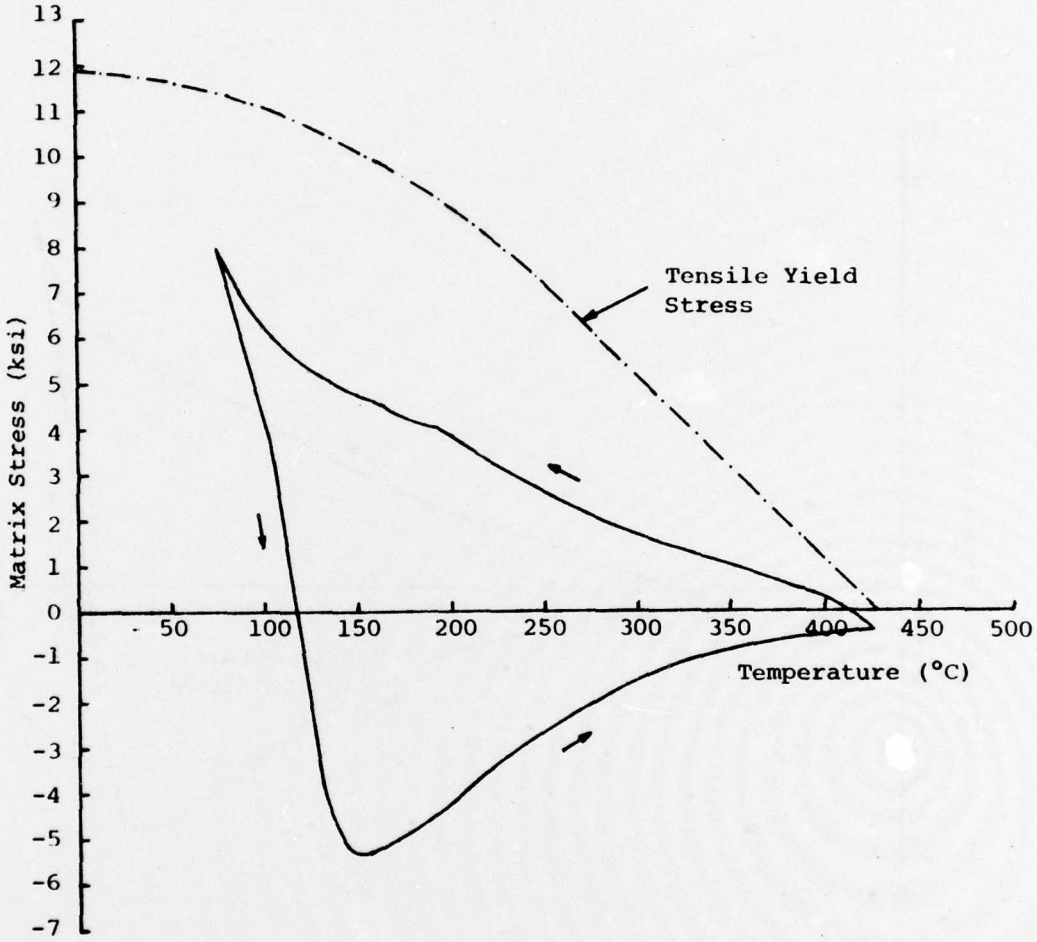

Figure 22. The matrix stress during thermal cycling of 2024 aluminum-boron, 6 minutes/cycle.

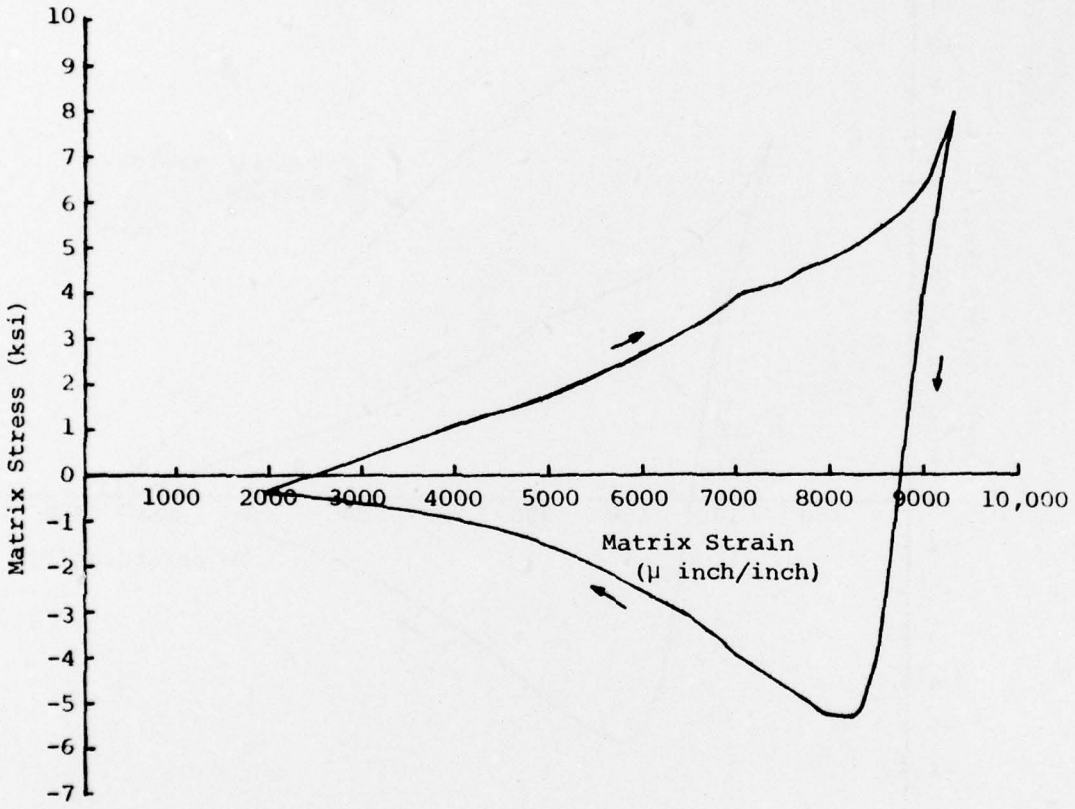

Figure 23. The matrix stress-strain curve during thermal cycling of 2024 aluminum-boron, 6 minutes/cycle.

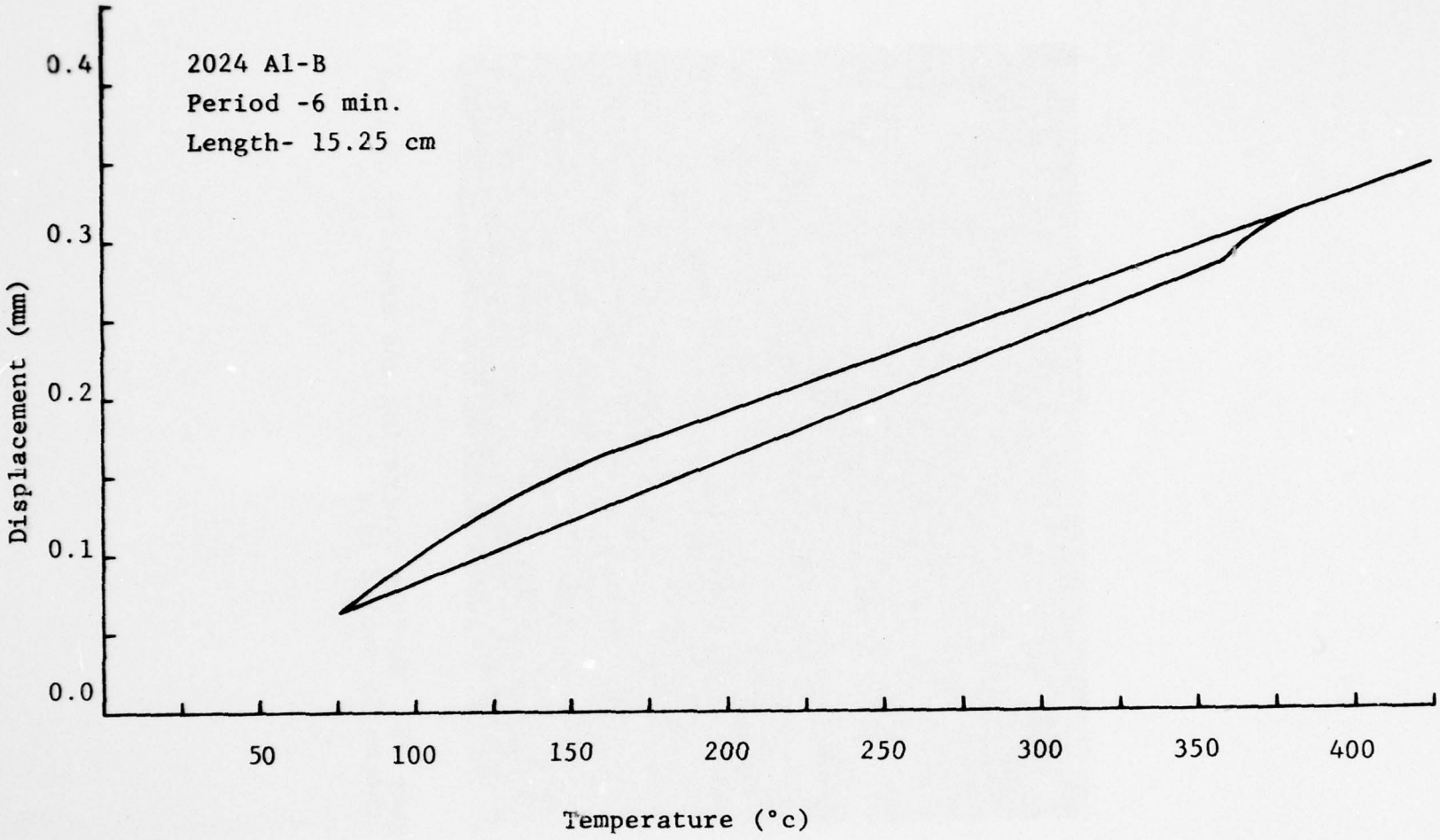

Figure 24. Calculated Composite Thermal Extension, 6 minutes/cycle.

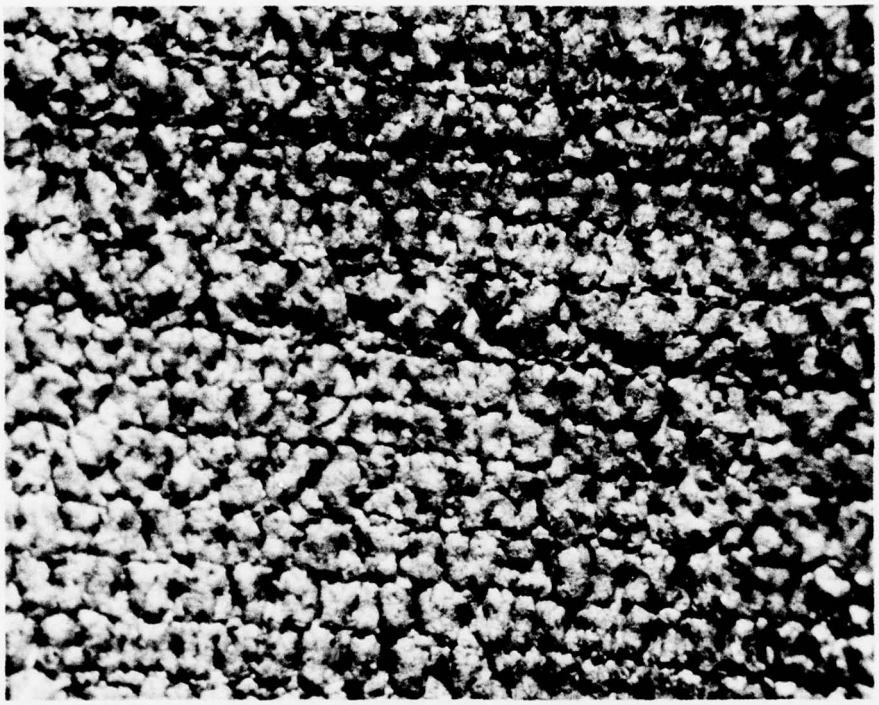

Figure 25. Surface roughening and cracking of B-Al thermally cycled in air.

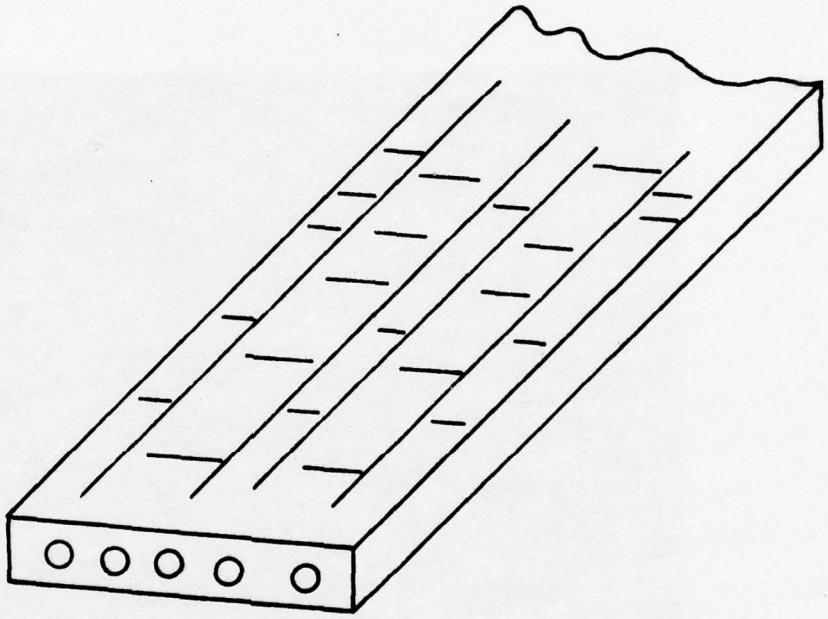

Figure 26. Diagramatic Representation of the Surface of a thermally cycled specimen.

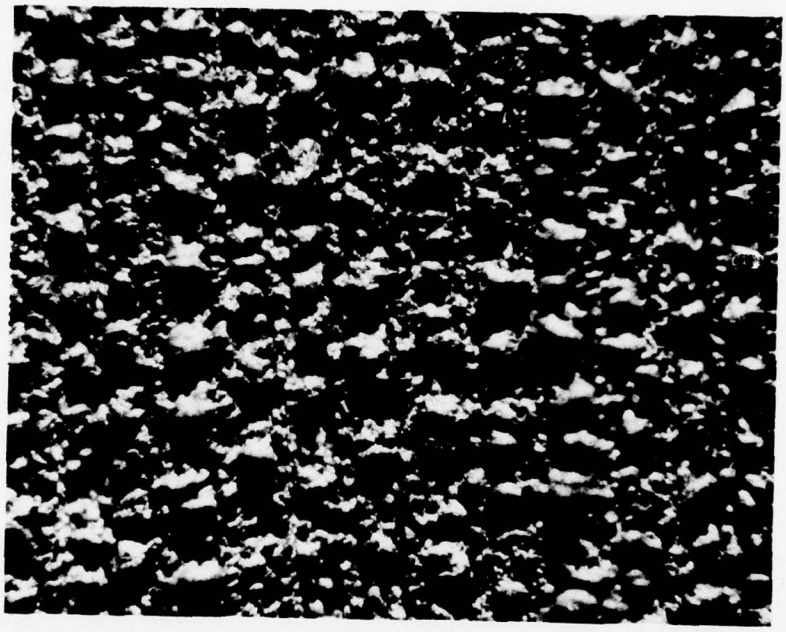

Figure 27. The spheroidazation of a thermally cylced boron-aluminum surface.

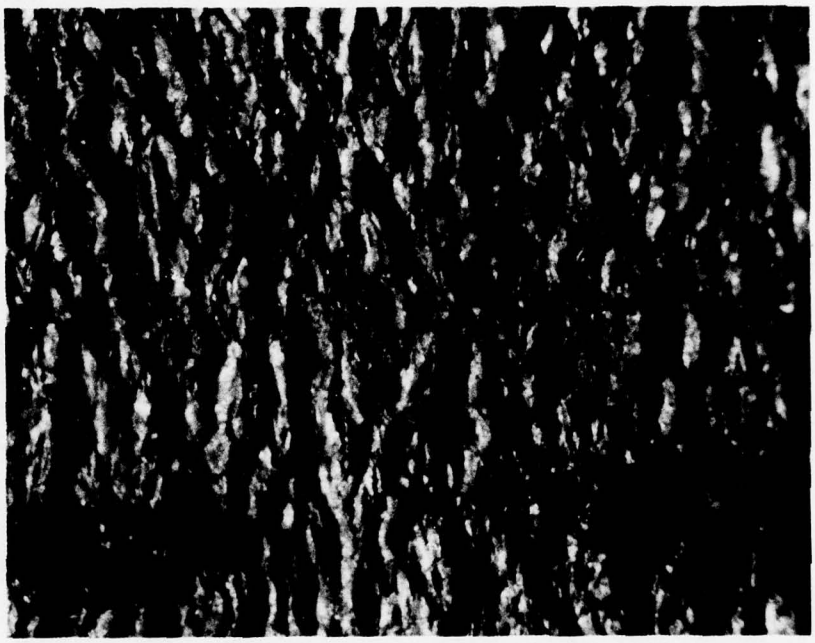

Figure 28. Surface disruption of thermally cycled carbon-aluminum composite.

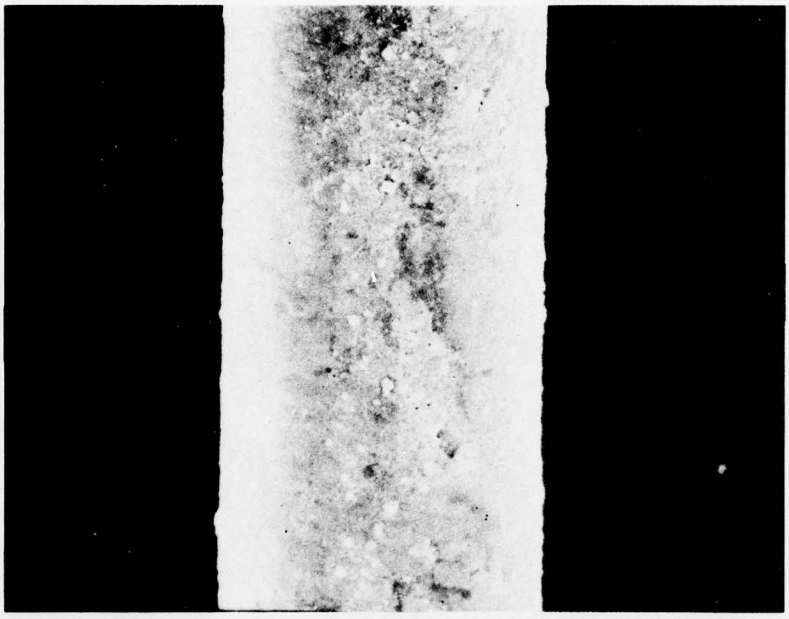

Figure 29. Reaction products on a boron fiber extracted after thermal cycling.

1. REPORT NUMBER	2. GOVT ACCESSION NO.	3. RECIPIENT'S CATALOG NUMBER
		(9)

4. TITLE (and Subtitle)
Investigations into the Mechanisms of Thermal Cycling Damage in Metal Matrix Composites

5. TYPE OF REPORT & PERIOD COVERED
Technical Report - 1 Jul 75-30 Jun 76
July 1, 1975 June 30, 1976

6. PERFORMING ORG. REPORT NUMBER
Met-E-761

7. AUTHOR(s)
Marvis K. White, Maurice M.A. Wright

8. CONTRACT OR GRANT NUMBER(s)
N00014-75-C-0352
NR 031-760

9. PERFORMING ORGANIZATION NAME AND ADDRESS
University of Tennessee Space Institute
Tullahoma, Tenn. 37388

10. PROGRAM ELEMENT, PROJECT, TASK AREA & WORK UNIT NUMBERS

11. CONTROLLING OFFICE NAME AND ADDRESS
Department of the Navy
Office of Naval Research
Washington, D.C. 20360

12. REPORT DATE
January, 1977 (11) Dec 76

13. NUMBER OF PAGES
84 (12) 90p.

14. MONITORING AGENCY NAME & ADDRESS *(if different from Controlling Office)*

15. SECURITY CLASS. *(of this report)*
unclassified

15a. DECLASSIFICATION/DOWNGRADING SCHEDULE

16. DISTRIBUTION STATEMENT *(of this Report)*
Reproduction in whole or in part is permitted for any purpose of the United States Government. Distribution unlimited.

17. DISTRIBUTION STATEMENT *(of the abstract entered in Block 20, if different from Report)*

18. SUPPLEMENTARY NOTES

19. KEY WORDS *(Continue on reverse side if necessary and identify by block number)*
Composites
Thermal Fatigue
Fracture
Fracture Mechanics

20. ABSTRACT *(Continue on reverse side if necessary and identify by block number)*

The mechanical properties of 6061, 2024, and 1100 aluminum reinforced with boron fibers were measured after 6000 thermal cycles in argon and in air between ambient temperature and 425°C. The cyclic periods used were 6 and 12 minutes in argon and 12 minutes in air. Fiber strengths were also measured before and after cycling. → next page

Little or no longitudinal strength degradation was evidenced by those materials cycled in argon while those cycled in air under otherwise identical

DD FORM 1 JAN 73 1473 EDITION OF 1 NOV 65 IS OBSOLETE
S/N 0102-014-6601

408 962

SECURITY CLASSIFICATION OF THIS PAGE (When Data Entered)

6pg

20. conditions showed greater than 50% strength reductions. Cycling in air produced lower transverse strengths than did cyling in argon. Fibers extracted from argon cycled specimens showed little or no loss of strength while those from air cycled specimens had large strength degradations.

The stresses and strains generated in a composite during thermal cycling were calculated in order to determine the nature of the strains producing matrix ratcheting and cracking. These calculations showed that large cyclic creep strains exist which relieve thermal stresses and prevent significant time independent plastic deformation.

Expansion measurements of the three boron-aluminum composites were made during thermal cycling in order to check the calculations and to provide further information on the deformation processes.

The effect of applied tensile stresses on the thermal cycling response of boron-aluminum in air was investigated. Tests using a variety of loads showed little or no effect of applied stress.

Also, the effect of reducing the cyclic temperatures was investigated. Keeping the cyclic period and temperature range the same as before, the lower and upper limits were shifted down to -100°c and 275°c. Matrix roughening was evidenced after 3000 cycles but no strength reduction was found.

In addition, thermal cycling tests were conducted on carbon-aluminum composites. 2024 aluminum composites containing 27 v/o thermal -50 fibers were thermally cycled between room temperature and 365°c and 425°c. All tests were done with a 3 minute cycle. Large amounts of surface roughening and cracking, a large but misleading decrease in flexual modulus, no change in the tensile modulus, and tensile strength reductions as high as about 70% were found using a maximum temperature of 425°c. No damage was indicated in those specimens cycled to a maximum temperature of 365°c.